A NEUROGENIC GENE EXPRESSION SIGNATURE SUPPORTS HUMAN THERMOGENIC ADIPOSE TISSUE DEVELOPMENT IN VIVO.

Javier Solivan-Rivera[1], Zinger Yang Loureiro[1], Tiffany DeSouza, Anand Desai, Qin Yang[1], Raziel Rojas-Rodriguez, Pantos Skritakis, Shannon Joyce, Denise Zhong, Tammy Nguyen[2,4], and Silvia Corvera[3,4,5]

[1]Morningside Graduate School of Biomedical Sciences, UMass Chan Medical School

[2]Department of Surgery, Division of Vascular Surgery, UMass Memorial Medical Center

[3]Program in Molecular Medicine, UMass Chan Medical School

[4]Diabetes Center of Excellence, UMass Chan Medical School

[5]Corresponding author at: silvia.corvera@umassmed.edu

Program in Molecular Medicine

373 Plantation Street

Worcester, MA 01605

ABSTRACT

Human beige/brite thermogenic adipose tissue exerts beneficial metabolic effects and may be harnessed to improve metabolic health. To uncover mechanisms by which thermogenic adipose tissue is generated and maintained we developed a species-hybrid model in which human mesenchymal progenitor cells are induced in vitro to differentiate into white or thermogenic adipocytes and are then implanted into immuno-compromised mice. Upon implantation, thermogenic adipocytes form a more densely vascularized and innervated adipose tissue compared to non-thermogenic adipocytes. Mouse endothelial and stem/progenitor cells recruited by implanted human thermogenic adipocytes are also qualitatively different, with differentially expressed genes mapping predominantly to circadian rhythm pathways. We trace the formation of this enhanced neurovascular architecture to higher expression of a distinct set of genes directly associated with neurogenesis (*THBS4*, *TNC*, *NTRK3* and *SPARCL1*), and to lower expression of genes associated with neurotransmitter degradation (*MAOA, ACHE)* by adipocytes in the developed tissue. Further analysis reveals that MAOA is abundant in human adipocytes but absent in mouse adipocytes, revealing species-specific mechanisms of neurotransmitter tone regulation. In summary, our work discovers specific neurogenic genes associated with development and maintenance of human thermogenic adipose tissue, reveals species-specific mechanisms of control of neurotransmitter tone, and suggests that targeting adipocyte MAOA may be a strategy for enhancing thermogenic adipose tissue activity in humans.

INTRODUCTION

A positive association between thermogenic "beige/brite" adipose tissue and metabolic health in humans has been repeatedly observed [1-4], and multiple studies have shown that human thermogenic adipocytes transplanted into mice affect whole-body metabolism [5, 6]. These studies provide evidence for a cause-effect relationship and a rationale for enhancing the activity and/or abundance of thermogenic adipose tissue as a therapeutic approach to metabolic disease. However, the cellular and molecular mechanisms by which human thermogenic adipose tissue develops and is maintained are largely unknown.

Accrual of new thermogenic adipose tissue can be stimulated by chronic cold exposure, extensive skin burns, and catecholamine producing tumors [7-9], all of which can acutely activate existing thermogenic adipocytes [10, 11]. Formation of new thermogenic adipose tissue must involve the generation of new adipocytes expressing the characteristic mitochondrial uncoupling protein 1 (UCP1), and the dense

vasculature and innervation that distinguishes thermogenic from white adipose tissue [12-15]. Increased vascular density is required to facilitate oxygen consumption and heat dissipation, and increased innervation sustains thermogenesis through sympathetic signaling [13]. The concurrence of three processes; new adipocyte differentiation, vascularization, and innervation, makes it difficult to determine which occurs first, and possible interdependencies. One possibility is that activation of thermogenic adipocytes results in the secretion of factors that induce vascularization and innervation [16]. Adipocyte progenitor cells within the newly forming vasculature could then differentiate into new thermogenic adipocytes [17, 18]. Alternatively, a direct effect of catecholamines on the vasculature might trigger angiogenesis, and beige adipocyte development from perivascular progenitor cells might ensue [19]. Understanding these dynamic, interrelated mechanisms of thermogenic adipose tissue development in humans is further hindered by limited models available.

Our laboratory has developed methods to obtain large numbers of mesenchymal progenitor cells from human adipose tissue and shown that these can give rise to multiple adipocyte subtypes [18]. Moreover, these cells can be implanted into immunocompromised mice, where they develop functional adipose tissue depots [20]. We reasoned that this cell implantation model, by clearly separating the adipocyte component (human) from vascular and neuronal components (mouse), could help deconvolve mechanisms of development and maintenance of human thermogenic adipose tissue. Using a combination of imaging and species-specific expressed genome analyses, we find that implanted human adipocytes continue to develop and maintain species and condition-specific specific features, where white and thermogenic adipocytes form depots characterized by a quantitatively and qualitatively distinct innervation and vascularization. We trace the mechanism by which adipocytes establish distinct fat depots to differential expression of genes involved in paracrine signaling and modulation of neurotransmitter tone. Notably, the expression of MAOA, which catalyzes the oxidative deamination and inactivation of multiple neurotransmitters, differs markedly between mice and human cells, highlighting the relevance of this hybrid model to understanding species-specific variations and providing insight into potential strategies to enhance adipose tissue thermogenesis in humans.

RESULTS

Formation of functional adipose depots from thermogenic versus non-thermogenic adipocytes.

To generate cells for implantation we derived mesenchymal progenitors from human subcutaneous adipose tissue [20] as detailed in Materials and Methods, and cell suspensions were injected subcutaneously into each flank of nude mice (Extended Figure 1 A,B). Discernible adipose tissue pads, and circulating human adiponectin, were detected in all mice (Extended Figure 1 C,D), demonstrating that human adipocytes were able to secrete characteristic adipokines for an extended period after implantation. To monitor the development of adipocytes within the in vivo environment, we performed immunohistochemistry of the excised tissue with an antibody to perilipin 1 (PLIN1), which delineates lipid droplets. This analysis revealed a progressive increase in lipid droplet size over a period of 16 weeks (Fig. 1A). Notably, implanted adipocytes grew larger than those in endogenous mouse subcutaneous white adipose tissue as early as week 4 after implantation, and continued to increase to match the mean size of adipocytes in the human tissue from which progenitor cells were obtained (Fig. 1A,B). The change in mean adipocyte size was mostly attributable to a shift from multilocular to unilocular adipocytes (Fig. 1C). Expression of human *PLIN1* gene was relatively stable from weeks 4 to 16 (Fig. 1D, top panels), but *ADIPOQ* expression decreased as adipocyte size increased (Fig 1D, lower panels), mimicking the known inverse correlation seen in humans between ADIPOQ production and adipocyte hypertrophy [21]. Importantly, there was no detectable expression of mouse *Plin1* or *Adipoq*, (Fig. 1D, top and lower panels), indicating that adipocytes in the developed depot are exclusively of human origin. These results indicate that as adipocytes continue to develop in the mouse they retain fundamental features of human adipose tissue, reflected by adipocyte size and regulated adiponectin expression.

We then asked whether depots formed from white (**W**hite **IM**planted=**WIM**) or thermogenically-induced adipocytes (**T**hermogenic **IM**planted=**TIM**) would be distinguishable from each other. The macroscopic features and weight of TIM and WIM were similar (Fig. 1E,F), as was the average concentration of circulating human adiponectin in mice harboring TIM compared to WIM (Fig. 1G). However, multilocular adipocytes could be detected in wholemount staining of TIM, by either PLIN1 immunostaining of whole mounts (Figure 1H, top panels, white arrows) or by H&E staining of tissue sections (Fig. 1H, lower panels, black arrows). Droplet quantification revealed a significant difference in mean droplet size (Fig. 1I), resulting from a higher density of small droplets (Fig. 1J). Expression of human *UCP1* was significantly higher in TIM (Fig. 1K), and expression of *LINC00473*, a marker for human thermogenic adipocytes [22], was exclusively detected in TIM (Fig. 1L). These results indicate that thermogenic features are maintained for a minimum of 8 weeks in adipose tissue developed from implanted cells.

Beige adipocytes induce development of adipose tissue with a denser neurovascular architecture

To analyze the development of vasculature we stained whole-mounts and thin sections from the excised implants with endothelial stain isolectin (Fig. 2A). We detected dispersed endothelial cells as early as week 2 after implantation in whole-mount specimens (Figure 2A, top panels). Between weeks 4 and 8, a well-developed vascular network, closely resembling that seen in human adipose tissue, was established. Vessels formed in apposition to enlarging adipocytes, as seen in sections co-stained with isolectin and antibodies to PLIN1 (Fig. 2A, lower panels). Quantification of the total intensity of isolectin staining in the thin sections, relative to PLIN1 staining to account for adipocyte mass, did not differ in a statistically significant way over time (Fig. 2B). However, quantification of the mean size of vascular structures stained by isolectin revealed a significant increase between weeks 4 and 8 (Fig. 2C), corresponding with the appearance of discernible vessels. Consistent with the intensity of isolectin staining, the expression of mouse vascular endothelial cadherin (*Cdh5*) did not differ in a statistically significant way over time, and was exclusively of mouse origin as human *CDH5* was undetectable (Fig. 2D). These results suggest that endothelial cells invade the emerging tissue early in development, and subsequently mature into morphologically discernable vessels. Despite the fact that all vasculature was of mouse origin, the vascular network was morphologically indistinguishable from human WAT (Fig 2A, comparing Week 16 with human adipose tissue (Human AT)).

We then compared the development of tissue vasculature between TIM and WIM after 8 weeks of implantation (Fig. 2E). Total intensity of isolectin staining in thin sections, relative to adipocyte mass as estimated by PLIN1 staining, was increased in TIM (Fig. 2F), as was the non-normalized intensity of isolectin in whole-mount specimens (Fig. 2G). The overall morphology of vascular structures was not different between WIM and TIM (Fig. 2H), suggesting that vessel maturation was unaffected. Gene expression levels of *Cdh5* were higher in TIM (Fig 2I), but those of human adipocyte genes *ADIPOQ* or *PLIN1*, were not different (Fig. 2J). These results indicate that thermogenic adipocytes induce the formation of a denser vascular network compared to non-thermogenic cells. We next asked whether TIM would have higher content of blood cells, which we would expect if the newly formed vascular network was functional. For this we measured content of blood cells in the developing tissue, using the hematopoietic cell marker CD45 and the macrophage marker F4/80. We find that TIM had significantly higher number of macrophages compared to WIM (Extended Figure 2), consistent with a denser, functional vascular network.

Sympathetic innervation often accompanies vascularization [23-25]. To determine whether beige adipocytes also promote enhanced sympathetic nerve recruitment, we co-stained implants to simultaneously detect tyrosine hydroxylase (TH) and isolectin. Punctate staining consistent with nerve terminals was detected in all implants, with some overlapping with isolectin (Fig. 2K). Quantification revealed significantly higher TH staining in TIM compared to WIM (Fig. 2L), indicating enhanced sympathetic recruitment in conjunction with enhanced vascularization.

The neurovascular network differentially responds to implanted adipocytes and supports TIM thermogenic phenotype.

To determine the extent to which the neurovascular network elicited by thermogenic adipocytes contributes to the maintenance of their phenotype, we examined the autonomous capacity of adipocytes to retain thermogenic gene expression. We compared adipocytes that were never stimulated to adipocytes that were chronically stimulated with Forskolin (Fsk), and with adipocytes from which Fsk was withdrawn after a period of chronic stimulation (Fig. 3A). Removal of Fsk from chronically stimulated adipocytes resulted in a rapid increase in droplet size, which reached the size seen in cells that were never exposed to Fsk within days of removal (Fig. 3B,C). Forskolin withdrawal also resulted in a sharp decrease in *UCP1*(Fig 3D) and *LINC00473* (Fig. 3E) expression, with values becoming statistically non-different from non-induced adipocytes within 5 days of withdrawal. Interestingly, the expression of *LINC00473* decreased even in the presence of chronic Fsk stimulation, while *UCP1* levels continued to increase over time, revealing different pathways of adaptation to chronic stimulation. Irrespective of these gene-specific differences, these results indicate that the thermogenic phenotype of adipocytes in-vitro is completely reversed within days of withdrawal of stimulation. We conclude that adipocytes lack the capacity to autonomously maintain a thermogenic phenotype, and that vascularization and innervation generated following implantation are likely to play a critical role in sustaining their thermogenic properties.

Conversely, the interactions between implanted adipocytes and the neuro-vasculature might have systemic effects. To examine this possibility, we examined host adipose depots. The weights of mouse inguinal white and interscapular brown adipose tissue (iWAT and iBAT, respectively) were similar between mice implanted with either WIM or TIM (Fig. 3F), but the iWAT, which in athymic nude mice is noticeably beige, looked 'whiter' in mice harboring TIM compared to WIM (Fig. 3G). This morphological difference correlated with lower *Ucp1* expression in iWAT of TIM-implanted mice, while no differences were

observed in iBAT (Fig. 3H). These results suggest that newly formed hybrid depots participate in feedback mechanisms that regulate total body content of thermogenic adipose tissue [26], potentially through their neurovascular architecture [27].

Distinct gene expression features of adipocytes and host cells in WIM and TIM

To explore underlying mechanisms by which thermogenic adipocytes elicit a different vascularization and innervation and control systemic thermogenic adipose tissue, we performed RNA sequencing on WIM and TIM after 8 weeks of implantation. To distinguish transcriptomes corresponding to either mouse or human cells, fastq files were aligned to both genomes, and resulting reads were classified as either of human or mouse origin using the XenofilteR R-package. We then used mouse transcriptomic data to infer the mouse cell types that comprise WIM and TIM (Fig 4A). As a framework we used single-cell datasets from Burl et al. [28], who profiled stromovascular cells from both inguinal and gonadal mouse depots. Consistent with their findings, we distinguish 9 clusters, corresponding to adipose stem cells at distinct stages of differentiation, vascular endothelial cells, vascular smooth muscle cells, lymphocytes, dendritic cells, macrophages, neutrophils, and an unidentified cluster (Fig 4B). The most prominent host-derived cell populations in WIM and TIM, predicted by dampened weighted least squares deconvolution (DWLS, https://github.com/dtsoucas/DWLS), were adipose stem/progenitor cells, macrophages, and vascular endothelial cells, with vascular smooth muscle cells, dendritic cells, and other immune cells at very low numbers. No detectable differences in the relative proportion of cell types were observed between WIM and TIM (Fig 4C). It is interesting to note that progenitor cells accompanying vascularization of the developing tissue did not differentiate into adipocytes, as the expression of mouse *Plin1* and *Adipoq* in WIM and TIM is negligible (Fig. 2I).

We then probed for expression level differences in mouse genes between WIM and TIM. Of 13,036 detected genes, 86 were higher in TIM (range 1.25- to 414-fold), and 124 genes were higher in WIM (range 1.25- to 8-fold), with a p-adjusted value lower than 0.05 (Fig 4D and Supplementary Table 1). Pathway analysis of all differentially expressed genes revealed circadian clock genes as the most prominent pathway, with higher expression in TIM of *Npas2* and *Arntl* (3.9- and 3.5-fold higher in TIM, padj values 9.39E-05 and 7.36E-06 respectively) and higher expression in WIM of *Dbp*, *Ciart*, *Per2* and *Per3* (3.1-, 2.9-, 2.8- and 2.4-fold, padj values 1.28E-20, 0.008, 1.22E-11 and 4.99E-08 respectively). We also find enrichment in cholesterol biosynthetic and extracellular matrix remodeling pathways (Fig. 4E). We then asked whether

differentially expressed genes correspond to a specific cell type, by searching for their expression in stromovascular cells from both inguinal and gonadal mouse depots shown in Figure 4B. Some of the differentially expressed genes associated with circadian rhythms (e.g. *Dbp*, *Per3*) or extracellular matrix remodeling (e.g. *Adamts4*, *Col4a2*) could be detected within clusters corresponding to progenitor cells and vascular endothelial cells (Fig. 4F). Genes in the cholesterol biosynthesis pathway (*Fdps* and *Cyp51*) are also seen in clusters corresponding to dendritic cells and macrophages. These results suggest that progenitor and endothelial cells respond to the different signals emanating from thermogenic versus non-thermogenic adipocytes, and adopt a specific functional phenotype.

To elucidate mechanisms by which human thermogenic and non-thermogenic adipocytes might induce differences in vascularization and innervation, we searched for genes differentially expressed between WIM and TIM that mapped to the human genome. Of 9655 detected genes, 515 were higher in WIM and 218 were higher in TIM, with a p-adjusted value lower than 0.05 (Fig. 4G, Supplementary Table 2). The most highly differentially expressed genes were associated with neurogenesis, including higher expression in TIM of *THBS4*, *TNC*, *SPARCL1* and *NTRK3* (5.6-, 2.7-, 2.7- and 2.4- fold, padj-values 0.006, 0.0003, 9.3E-09, and 0.0001, respectively) [29-34]. Pathway analysis of genes with higher expression in TIM (Fig 4H) revealed enrichment in ribosomal protein-encoding genes, suggesting higher protein synthesis activity, followed by pathways affecting extracellular matrix composition, including numerous collagens. Many of these genes have been implicated in the control of blood vessel development, and could underlie the increased vascular density seen in TIM. As expected, *UCP1* mean values were higher in TIM (18.2 and 42.3 in WIM and TIM, respectively), consistent with the significantly elevated *UCP1* expression seen by RT-PCR (Fig 1K). Genes expressed at higher levels in WIM were associated with cholesterol and lipid metabolism as well as insulin action (Fig 4I), consistent with a more prominent role for lipid storage pathways in non-thermogenic adipocytes as they develop in vivo.

To identify genes that might be most relevant to the maintenance of the thermogenic phenotype, we searched for genes differentially expressed between non-thermogenic and thermogenic adipocytes prior to implantation that remain differentially expressed after 8 weeks. 988 genes were more highly expressed in thermogenic adipocytes, and 729 more highly expressed in non-thermogenic adipocytes (>2-fold, p-adjusted values < 0.05; Fig. 5A, Supplementary Table 3). Genes were assigned to Gene Ontology (GO) categories using https://go.princeton.edu/cgi-bin/GOTermMapper, a tool for mapping granular GO annotations to a set of broader, high-level GO parent terms [35]. Genes in thermogenic adipocytes

disproportionally mapped to GO categories associated with secretion (Fig. 5B), and were enriched in pathways of extracellular matrix organization and signaling through GPCRs and IGFs (Fig 5C). Genes that were up-regulated in non-thermogenic adipocytes were enriched in lipid metabolism pathways and transcriptional control of adipogenesis (Fig 5D). Of the 988 genes that were more highly expressed in thermogenic adipocytes prior to implantation, 21 were more highly expressed in TIM compared to WIM after 8 weeks (Supplementary Table 4), and 6 of these (*MMP14*, *ADAM19*, *TNC*, *ELN*, *COL12A1* and *TGFB3*) are associated with extracellular matrix organization, which was the only pathway enriched by these genes (Fig. 5E). Of the 729 genes that were expressed at higher levels in non-thermogenic adipocytes prior to implantation, 28 remained higher in WIM compared to TIM (Supplementary Table 4). Pathway analysis of these genes revealed neurotransmitter clearance as the top enriched pathway, with 2 genes, *ACHE* and *MAOA*, being higher in WIM.

A lower expression of *ACHE* and *MAOA* in adipocytes would be expected to enhance neurotransmitter tone and maintenance of the thermogenic phenotype. Indeed, in mouse models, Maoa activity has been implicated in the regulation of norepinephrine stimulated adipose tissue lipolysis and browning, but its expression has been localized to a specific macrophage population [36-38]. Our finding of *MAOA* transcripts in WIM and TIM suggested expression in human adipocytes. To confirm that *MAOA* transcripts are indeed present in adipocytes in endogenous human adipose tissue, we re-analyzed single-nuclei RNA Seq data generated by Sun et. al. [39]. We reproduced their main findings, including the presence of a large proportion of immune cells, and a clearly defined adipocyte population (Fig. 6A). *MAOA* transcripts were detected exclusively in the population of cells also expressing *ADIPOQ*, which correspond to adipocytes (Fig. 6B). Adipocyte, smooth muscle cells and fibroblast nuclei also contained transcripts for *SLC22A3*, the major extra-neuronal catecholamine transporter, indicating that human adipocytes express both genes required for norepinephrine clearance. In contrast, neither *Maoa* nor *Slc22a3* transcripts were detectable in single cells expressing *Adipoq* from the data of Burl et al. [28] (Figure 6C). To confirm that transcriptional profiles reflect protein levels, we conducted parallel RT-PCR and western blotting analysis of human adipocytes at different stages of differentiation in vitro, and find a close correlation between *MAOA* mRNA and protein levels (Figure 6D and E). To verify that MAOA protein expression in adipocytes is indeed species-specific, we stained sectioned human adipose tissue, mouse adipose tissue and WIM with species-specific antibodies to PLIN1/Plin1 and MAOA/Maoa. We detected PLIN1/Plin1 in all tissues, but MAOA/Maoa was exclusively detected in adipocytes from human adipose tissue and WIM (Figure 6F).

DISCUSSION

The abundance of thermogenic adipose tissue in human adults has been shown to be closely correlated with metabolic health [2-4, 40], and transplantation of brown fat, genetically engineered human adipocytes, or primary "beige" adipocytes into mice results in improvement of glucose homeostasis [6, 41-44], demonstrating a cause-effect relationship. These studies have catalyzed efforts to understand the specific features of thermogenic adipose tissue that can be leveraged to improve human health. These efforts are limited by the difficulty of accessing thermogenic adipose tissue from human subjects, and depend largely on studies in mouse models. In this paper, we used a species-hybrid model of adipose tissue development, in which adipose depots are formed after implantation of developing human adipocytes into mice. Our model is enabled by previously described methods by which large numbers of multipotent progenitor cells can be produced from small samples of human adipose tissue, which can be driven in vitro towards differentiation into multiple adipocyte subtypes [18], and fully mature when transplanted into the in vivo environment [20].

While adipocytes occupy the majority of the volume of mature adipose tissue, they comprise only about 50% of its cells, the remaining corresponding to cells of the vascular, neural and immune systems [45]. Our model allows us to distinguish adipocytes from other cellular components at the transcriptional level, and transcriptomic data can be complemented with single cell atlases [45-47]to discern features of different cell types during tissue development and thermogenic adipose tissue maintenance. Salient among the multiple findings of this study are, first, that adipocyte size is strictly genetically determined, as implanted developing adipocytes reached the size of those in the adipose tissue of the donor from which the progenitors were obtained, which was significantly larger than adipocytes in any of the host mouse depots. Second, we find that the neurovascular network induced by thermogenic adipocytes is quantitatively and qualitatively different from that induced by non-thermogenic adipocytes and is essential for maintenance of the thermogenic phenotype. Third, we find that the most significant pathways in adipocytes associated with maintenance of the thermogenic phenotype are increased expression of neurogenic factors, and decreased expression of neurotransmitter clearance enzymes. One of these, MAOA, is expressed in human but not mouse adipocytes, revealing critical species-dependent differences of thermogenic adipose tissue control.

The cellular mechanisms that lead to the formation of a mature vascular network involve chemotactic, haptotactic, and mechanotactic stimuli that initiate migration of endothelial cells followed by their organization into mature tubular structures [48]. Our results indicate that this process is initiated by developing adipocytes, as infiltration by endothelial cells precedes the formation of blood vessels within the maturing tissue. Importantly, the vascular network recruited by thermogenic adipocytes is both quantitatively and qualitatively different than that recruited by non-thermogenic adipocytes. A denser vascular network is seen in TIM, and vascular endothelial cells displayed a significant increase in *Col4A2*, which is expressed by and associated with small vessel stability[49]. Another distinctive feature of vascular endothelial cells in TIM is the expression of lower levels of circadian clock genes, including *Dbp*, *Per2* and *Per3*, which have been seen to oscillate in adipose tissues of mice and humans, and to be affected by diet [50-53]. Our findings indicate that these genes are expressed in the vasculature of adipose tissue, rather than in the adipocytes, potentially explaining the parallel oscillations of these genes in multiple other peripheral tissues [54, 55]. Interestingly, Per3 has been reported to suppress adipogenesis by regulating Klf15 expression [53], and clock genes are associated with the activity of thermogenic adipocytes [56, 57]. The relative importance of stromovascular versus adipocyte-intrinsic oscillatory mechanism in regulating adipose tissue homeostasis will be important to discern in future studies.

In addition to host endothelial cells, human adipocytes recruit all other cells associated with the stromovascular fraction of adipose tissue, including progenitor cells and cells of the immune system. Notably the proportion of macrophages relative to other immune cells in WIM and TIM resembles the cellular composition of endogenous mouse adipose tissue, which differs from human adipose tissue in containing a higher proportion of macrophages [47]. These results suggests that the overall immune composition of adipose tissue is not dictated by the adipocytes, but by the other cells within the tissue such as endothelial or progenitor cells. Indeed, adipose progenitor cells are known to exert strong immunomodulatory effects which could influence the immune composition of the tissue [58, 59]. It is also interesting that adipose stem/progenitor cells from the host do not differentiate into adipocytes, as adipocytes in WIM and TIM matched the larger size of human adipose tissue from which progenitors were obtained, and all adipocyte-specific markers in WIM and TIM mapped to the human genome. These results indicate that adipocyte size is genetically defined, and also suggest that progenitor differentiation into new adipocytes may only occur under conditions in which systemic adipocyte capacity becomes insufficient, such as after prolonged high-fat diet [60].

The ability of implanted thermogenic adipocytes to recruit a specific neurovascular network is critical, as in the absence of external stimuli adipocytes lose their thermogenic phenotype within days, while within the mouse host it remains for over 8 weeks. The mechanisms by which thermogenic adipocytes maintain their phenotype in vivo are likely to be associated with innervation, as multiple studies have demonstrated that denervation results in a rapid loss of thermogenic adipose tissue features [13, 27]. Indeed, we find enhanced innervation in TIM, which is likely to contribute to the maintenance of the thermogenic phenotype. Mechanistically, thermogenic adipocytes express higher levels of secreted and extracellular matrix proteins, and after 8 weeks in vivo the most highly differentially expressed genes between WIM and TIM are associated with neurogenesis (*THBS4*, *TNC*, *NTRK3* and *SPARCL1*) [29-34]. Interestingly, Thbs4 and Sparcl1 have been identified as factors in blood from young mice that can directly stimulate synaptogenesis [29], and beige adipocytes have been found to be neuroprotective [61]. These results suggest that the neurogenic factors produced by thermogenic adipocytes might not only elicit local increases in innervation, but might more broadly contribute to production of blood factors involved in neuroprotection.

In addition to higher expression of neurogenic factors, thermogenic adipocytes also express lower levels of *MAOA* and *ACHE*. MAOA catalyzes the oxidative deamination of norepinephrine, and may thereby play a direct role in thermogenesis by dampening adrenergic tone. ACHE is responsible for the catabolism of acetylcholine, which has been found to activate thermogenic adipocytes in the subcutaneous adipose tissue of mice [62]. Indeed, Maoa has been implicated in the control of adipose tissue responsiveness to catecholamines in mice [36, 37], through its expression in a specific subset of macrophages. Our studies indicate that in humans, *MAOA* is strongly expressed in adipocytes, which also express the non-neuronal transporter *SLC22A3*, allowing for transport and degradation of catecholamines. These findings and those of others [63] suggest that adipocytes themselves play a major role in establishing adrenergic tone and controlling thermogenic activity. Consistent with this possibility are findings that MAOA is increased in visceral adipose tissue of obese compared to non-obese patients [64], which displays decreased expression of UCP1 [65-67]. Whether the observed upregulation of MAOA occurs in adipocytes within the visceral adipose tissue, and whether inhibition of the enzyme might prevent loss of thermogenic adipocytes, are important questions for future studies. If so, the development of non-CNS penetrable, adipocyte favoring formulations of MAOA inhibitors might have the potential to enhance thermogenic adipocyte mass and ameliorate metabolic disease.

MATERIALS AND METHODS

Human Subjects: Abdominal adipose tissue was collected from discarded tissue of patients undergoing panniculectomy, with approval from the University of Massachusetts Institutional Review Board (IRB ID 14734_13).

Generation of cells and implants: Small pieces of fat (~1mm^3) from the excised human adipose tissue were embedded in Matrigel (200 explants/10 cm dish) and cultured for 14 days as described before[20]. Single-cell suspensions were obtained using dispase and plated into 150 mm tissue culture dishes. After 72 h, cells were split 1:2, grown for an additional 72 h, recovered by trypsinization and frozen. To generate the implants, ~10E7 cells were thawed into each 150 mm plate, and after 72 hours split 1:2 at a dense seeding density of ~8E6 cells per 150 mm plate. Upon confluence (approximately 72 hours after plating), differentiation was induced by replacing the growth media with DMEM +10% FBS, 0.5 mM 3-isobutyl-1-methylxanthine, 1 μM dexamethasone, and 1 μg/mL insulin (MDI). MDI media was changed daily for 72 hours at which time the differentiation medium was replaced by DMEM + 10%FBS, 50% of which was replaced every 48 hours for 10 days. After 10 days of differentiation, a subset of cells was stimulated daily for 7 days with forskolin (1 μM final concentration) to induce the thermogenic phenotype. Single cell suspensions of differentiated and thermogenic-induced adipocytes were obtained by incubation for 7-10 min in Trypsin (1X)/collagenase (0.5 mg/mL). Proteases were quenched by dilution into culture media, cells pelleted by centrifugation at 500 rpm for 10 minutes. The media layer between floating and pelleted cells was removed, and remaining cells brought to 1 mL total volume with ice-cold PBS, placed on ice and mixed with an equal volume of ice-cold Matrigel. 0.5 mL aliquots of the cell suspension were placed in 1 ml syringes on ice, and injected subcutaneously into each flank of immunodeficiency male nude mice (Nu/J Jackson labs stock no: 002019) using a 20G needle. At each experimental time point, developed implants were dissected and snap frozen until further analysis.

Human-specific adiponectin ELISA: Blood was obtained through cardiac puncture, centrifuged, and the plasma was collected and stored at -80°C. A human-specific adiponectin ELISA (Invitrogen KHP0041) was used to measure the concentration of human adiponectin in mouse blood.

RNA extraction and quantitative PCR: Implants were placed on TRIzol (Invitrogen) and homogenized with Tissuelyser (Qiagen). Total RNA was reverse transcribed using the iScript™ cDNA Synthesis Kit

(BioRad) per manufacturer's protocol. Either SYBR Green or PrimePCR™ Probes (BioRad) were used to detect amplification of human- and mouse-specific genes using the following primers:

Primers	Forward	Reverse
Human RPL4	GCCTGCTGTATTCAAGGCTC	GGTTGGTGCAAACATTCGGC
Mouse Rpl4	CCCCTCATATCGGTGTACTCC	ACGGCATAGGGCTGTCTGT
Human PLIN1	ACCAGCAAGCCCAGAAGTC	CATGGTCTGCACGGTGTATC
Mouse Plin1	CTGTGTGCAATGCCTATGAGA	CTGGAGGGTATTGAAGAGCCG
Human CDH5	CTGCTGCAGGGTCTTTTTCT	AGGGCATGATGGTCAGTCTC
Mouse Cdh5	TACTCAGCCCTGCTCTGGTT	TGGCTCTGTGGTGCAGTTAC

RNA-Seq: RNA was extracted from white and thermogenic implants using the TRIzol method. Library preparation was performed using the TruSeq cDNA library construction (Illumina). Samples were processed on the Illumina HiSeq 550 sequencing system with the NextSeq 500/550 High Output kit v2.5 (Illumina, Cat. No. 20024906). The generated .fastq files were loaded into the DolphinNext platform (https://dolphinnext.umassmed.edu/) and the Bulk RNA sequencing pipeline was used. The .fastq files were aligned to both the human (hg38) and the mouse (mm10) genome. The resulting alignments were processed using the R-package XenofilteR in order to classify reads as either of human or mouse origin. Reference (https://github.com/PeeperLab/XenofilteR) for more details on XenofilteR source code. Once aligned, the files were run through RSEM for normalization. Differential expression analysis was performed using the DEBrowser platform (https://debrowser.umassmed.edu/). Gene ontology analysis was performed by combining results from TopFunn (https://toppgene.cchmc.org/).

***Single Cell RNA-Seq Processing*:** Single-cell RNA sequencing data was obtained from Burl, Rayanne B., et al. 2018. The provided .fastq files were loaded into DolphinNext and processed using the Cell Ranger pipeline. The output files from Cell Ranger were then loaded into the Seurat (https://satijalab.org/seurat/index.html). We removed unwanted cells from the data by sub-setting features as follow: nFeature_RNA > 100 & nFeature_RNA < 5000. We then proceeded to normalize the data using a logarithmic normalization method with a scale factor of 10000. We then applied a linear transformation to scale the data followed by dimension reduction analysis (PCA). Following PCA analysis we determined that the first 8 principal component analysis were optimal for further analysis. To cluster the cells, we performed non-linear dimension reduction analysis using the UMAP algorithm. Analysis was done using

the first 8 principal components and a resolution of 0.3. Finally, differentially expressed genes for each cluster were identified to determine biomarkers for cell cluster identification.

Cell Predictor Using DWLS Deconvolution: Source code for DWLS deconvolution can be found at https://github.com/dtsoucas/DWLS. Briefly, metadata from the Seurat object was used to generate a matrix containing the reads from the scRNA and one containing the cluster labels for each gene. A signature matrix was generated using the MAST function provided with the DWLS deconvolution code. Only genes in common between the scRNA and the bulk RNA dataset were used for prediction. DWLS deconvolution was performed using the solveDampenedWLS function and proportions of predicted cells were plotted.

Single Nuclei RNA-Seq Processing: Seurat objects for single nuclei RNA sequencing was kindly provided by the Wolfrum lab, who published their analysis[39]. Briefly, the Seurat objects containing the raw data were loaded the Seurat package, and two different samples were processed: single nuclei from human brown adipose tissue, single nuclei from mouse brown adipocytes. Briefly, for the human brown adipose tissue dataset, we first removed unwanted cells from the data by sub-setting features as follow: nCount_RNA > 1000 & nCount_RNA < 8000 & prop.mito < 0.3. We then normalized the data using a logarithmic normalization with a scale factor of 10000. We followed this by applying a linear transformation to scale the data followed by dimension reduction analysis (PCA). We determined that the first 10 principal component analysis were optimal for further analysis. To cluster the cells, we performed non-linear dimension reduction analysis using the UMAP algorithm. Analysis was done using the first 8 principal components and a resolution of 0.3. For the mouse brown adipocytes, we first removed unwanted cells from the data by sub-setting features as follow: nFeature_RNA > 1000 & nFeature_RNA < 5000. We then normalized the data using a logarithmic normalization with a scale factor of 10000. We followed this by applying a linear transformation to scale the data followed by dimension reduction analysis (PCA). We determined that the first 8 principal component analysis were optimal for further analysis. To cluster the cells, we performed non-linear dimension reduction analysis using the UMAP algorithm. Analysis was done using the first 8 principal components and a resolution of 0.2. Finally, clusters names were assigned using SingleR (https://github.com/dviraran/SingleR). The human primary cell atlas [68] was used as a reference to identify clusters based on differentially expressed genes of human brown adipose tissue.

Histochemistry and quantification: All samples were fixed in 4% paraformaldehyde overnight at 4°C and thoroughly washed with PBS. Tissue sections (8 μm) were mounted on Superfrost Plus microscope slides

(Fisher Scientific) and stained with hematoxylin and eosin. For whole-mount staining, tissue fragments (~1mm^3) were stained and mounted between 1.5 mm coverslips sealed with ProLong Gold Antifade Reagent (Life Technologies). Mouse vasculature was detected using isolectin GS-IB4 AlexaFluor-647 conjugate (Invitrogen I32450) and human vasculature using Ulex Europaeus Agglutinin I (UEA I), DyLight® 594 (Vector Laboratories DL-1067-1). Nuclei were stained using DAPI (Life Sciences 62249). Perilipin-1 was detected with an antibody that recognizes both human and mouse protein (CellSignaling #9349). MAOA was detected using CellSignaling #73030 (human) or CellSignaling #75330 (mouse). To identify sympathetic nerves an antibody for Tyrosine Hydroxylase was used (Millipore Sigma - AB152). Macrophages were identified by co-staining using antibodies for CD45 (Abcam – ab8216) and F4/80 (Abcam – ab6640). Tissue sections were imaged using ZEISS Axio Scan Z1. Whole-mount images were acquired using an Olympus IX81 microscope (Center Valley, PA) with dual Andor Zyla sCMOS 4.2 cameras (Belfast, UK) mounted on an Andor TuCam two camera adapter (Belfast, UK).

Image analysis was performed using the open software platform FIJI. For all images to be compared, a single stack was generated and subjected to the same filtering and quantification processes. Adipocyte area was determined from PLIN1 stained images imported as a single stack, converted to 8-bit grayscale, binarized, eroded twice, and object number and size measured through particle analysis (size = 350-2900 um, circularity = 0.25-1). Density distributions (scaled) were generated using R-studio through the density distribution function in ggplot2. Vascular density and size were measured using isolectin stained images, imported as a single stack into FIJI, background subtracted (rolling radius = 1) to enhance contrast, binarized using the Threshold function and subjected to particle analysis. The total vascular area of each section was the sum of the individual particles. The average vascular size was the mean of the individual particles. For macrophage quantification, CD45, F4/80 and DAPI images were background subtracted (rolling radius = 1) and binarized. To isolate macrophages that were both CD45 and F4/80 positive we used the image calculator function (image calculator > operation: AND). Particle analysis was performed and the number of particles normalized to the number of nuclei present in the whole section to account for differences in section sizes. Sympathetic density was calculated using TH and isolectin stained images after background subtraction (rolling radius = 1) and binarization. Total sympathetic area in the section was the sum of all particles normalized to the number of nuclei present in the whole section to account for differences in section sizes.

Thermogenic withdrawal of thermogenic adipocytes: Cells (~6.0×10^6) were thawed and seeded on 6-well plates, differentiated into white adipocytes and stimulated with forskolin as described above. After chronic forskolin stimulation, a subset of cells was removed from daily stimulation for 10 days. Images were taken and samples were placed on TRIzol (Invitrogen) at days 0, 2, 5, 7, and 10 of withdrawal. Samples were homogenized using the Tissuelyser (QIAGEN), and total RNA was then isolated for analysis as described above.

ACKNOWLEDGEMENTS

This study was supported by NIH grants DK089101 and DK123028 to SC and GM135751 to JSR. We acknowledge the use of services from the UMASS SCOPE core for high resolution confocal imaging, the biomedical imaging (BIG) facility for epifluorescence imaging and image analysis consultation. Finally, we acknowledge the use of services from the UMASS Morphology Core facility for sample preparation and sectioning for histological analysis.

AUTHOR CONTRIBUTIONS

JSR: hypothesis generation, conceptual design, experiment design and performance, data analysis, manuscript preparation. ZYL: conceptual design, experiment design and performance, data analysis, manuscript preparation. TD: experiment design and performance, data analysis, manuscript preparation. AD: experiment design and performance, data analysis, manuscript preparation. QY: conceptual design, manuscript preparation. RRR: conceptual design and performance. PS: conceptual design and performance. SJ: conceptual design, manuscript preparation. DZ: conceptual design, manuscript preparation. TN: conceptual design, manuscript preparation. SC: supervision of work, hypothesis generation, conceptual design, manuscript preparation.

DECLARATION OF INTERESTS

The authors declare no competing interests.

REFERENCES

1. Enerback, S., *Human brown adipose tissue.* Cell Metab, 2010. **11**(4): p. 248-52.

2. Virtanen, K.A., et al., *Functional brown adipose tissue in healthy adults.* N Engl J Med, 2009. **360**(15): p. 1518-25.

3. van Marken Lichtenbelt, W.D., et al., *Cold-activated brown adipose tissue in healthy men.* N Engl J Med, 2009. **360**(15): p. 1500-8.

4. Cypess, A.M., et al., *Identification and importance of brown adipose tissue in adult humans.* N Engl J Med, 2009. **360**(15): p. 1509-17.

5. Wang, C.H., et al., *CRISPR-engineered human brown-like adipocytes prevent diet-induced obesity and ameliorate metabolic syndrome in mice.* Sci Transl Med, 2020. **12**(558): p. eaaz8664.

6. Min, S.Y., et al., *Human 'brite/beige' adipocytes develop from capillary networks, and their implantation improves metabolic homeostasis in mice.* Nat Med, 2016. **22**(3): p. 312-8.

7. van der Lans, A.A., et al., *Cold acclimation recruits human brown fat and increases nonshivering thermogenesis.* J Clin Invest, 2013. **123**(8): p. 3395-403.

8. Sidossis, L.S., et al., *Browning of Subcutaneous White Adipose Tissue in Humans after Severe Adrenergic Stress.* Cell Metab, 2015. **22**(2): p. 219-27.

9. Dong, A., et al., *Hypermetabolic mesenteric brown adipose tissue on dual-time point FDG PET/CT in a patient with benign retroperitoneal pheochromocytoma.* Clin Nucl Med, 2014. **39**(3): p. e229-32.

10. Cypess, A.M., et al., *Activation of human brown adipose tissue by a beta3-adrenergic receptor agonist.* Cell Metab, 2015. **21**(1): p. 33-8.

11. Cypess, A.M., et al., *Cold but not sympathomimetics activates human brown adipose tissue in vivo.* Proc Natl Acad Sci U S A, 2012. **109**(25): p. 10001-5.

12. Francois, M., et al., *Sympathetic innervation of the interscapular brown adipose tissue in mouse.* Ann N Y Acad Sci, 2019. **1454**(1): p. 3-13.

13. Cao, Q., et al., *Sympathetic nerve innervation is required for beigeing in white fat.* Physiological Reports, 2019(6): p. e14031.

14. Chi, J., et al., *Three-Dimensional Adipose Tissue Imaging Reveals Regional Variation in Beige Fat Biogenesis and PRDM16-Dependent Sympathetic Neurite Density.* Cell Metab, 2018. **27**(1): p. 226-236 e3.

15. Sievers, W., et al., *Innervation of supraclavicular adipose tissue: A human cadaveric study.* PLoS One, 2020. **15**(7): p. e0236286.

16. Zhao, Y., et al., *Transient Overexpression of Vascular Endothelial Growth Factor A in Adipose Tissue Promotes Energy Expenditure via Activation of the Sympathetic Nervous System.* Mol Cell Biol, 2018. **38**(22): p. e00242-18.

17. Shao, M., et al., *Cellular Origins of Beige Fat Cells Revisited.* Diabetes, 2019. **68**(10): p. 1874-1885.

18. Min, S.Y., et al., *Diverse repertoire of human adipocyte subtypes develops from transcriptionally distinct mesenchymal progenitor cells.* Proc Natl Acad Sci U S A, 2019. **116**(36): p. 17970-17979.

19. Lee, Y.H., et al., *Cellular origins of cold-induced brown adipocytes in adult mice.* FASEB J, 2015. **29**(1): p. 286-99.

20. Rojas-Rodriguez, R., et al., *Generation of Functional Human Adipose Tissue in Mice from Primed Progenitor Cells.* Tissue Eng Part A, 2019. **25**(11-12): p. 842-854.

21. Robciuc, M.R., et al., *VEGFB/VEGFR1-Induced Expansion of Adipose Vasculature Counteracts Obesity and Related Metabolic Complications.* Cell Metab, 2016. **23**(4): p. 712-24.

22. Tran, K.V., et al., *Human thermogenic adipocyte regulation by the long noncoding RNA LINC00473.* Nat Metab, 2020. **2**(5): p. 397-412.

23. Carmeliet, P., *Blood vessels and nerves: common signals, pathways and diseases.* Nat Rev Genet, 2003. **4**(9): p. 710-20.

24. Pellegrinelli, V., et al., *Adipocyte-secreted BMP8b mediates adrenergic-induced remodeling of the neuro-vascular network in adipose tissue.* Nat Commun, 2018. **9**(1): p. 4974.

25. Reinert, R.B., et al., *Vascular endothelial growth factor coordinates islet innervation via vascular scaffolding.* Development, 2014. **141**(7): p. 1480-91.

26. Schulz, T.J., et al., *Brown-fat paucity due to impaired BMP signalling induces compensatory browning of white fat.* Nature, 2013. **495**(7441): p. 379-83.

27. Nguyen, N.L., et al., *Separate and shared sympathetic outflow to white and brown fat coordinately regulates thermoregulation and beige adipocyte recruitment.* Am J Physiol Regul Integr Comp Physiol, 2017. **312**(1): p. R132-R145.

28. Burl, R.B., et al., *Deconstructing Adipogenesis Induced by beta3-Adrenergic Receptor Activation with Single-Cell Expression Profiling.* Cell Metab, 2018. **28**(2): p. 300-309 e4.

29. Gan, K.J. and T.C. Sudhof, *Specific factors in blood from young but not old mice directly promote synapse formation and NMDA-receptor recruitment.* Proc Natl Acad Sci U S A, 2019. **116**(25): p. 12524-12533.

30. Girard, F., S. Eichenberger, and M.R. Celio, *Thrombospondin 4 deficiency in mouse impairs neuronal migration in the early postnatal and adult brain.* Mol Cell Neurosci, 2014. **61**: p. 176-86.

31. Tucic, M., V. Stamenkovic, and P. Andjus, *The Extracellular Matrix Glycoprotein Tenascin C and Adult Neurogenesis.* Front Cell Dev Biol, 2021. **9**: p. 674199.

32. Naito, Y., A.K. Lee, and H. Takahashi, *Emerging roles of the neurotrophin receptor TrkC in synapse organization.* Neurosci Res, 2017. **116**: p. 10-17.

33. Ramirez, J.J., D.S. Bindu, and C. Eroglu, *Building and destroying synaptic bridges: How do Hevin/Sparcl1, SPARC, and MDGAs modify trans-synaptic neurexin-neuroligin interactions?* Structure, 2021. **29**(7): p. 635-637.

34. Singh, S.K., et al., *Astrocytes Assemble Thalamocortical Synapses by Bridging NRX1alpha and NL1 via Hevin.* Cell, 2016. **164**(1-2): p. 183-196.

35. Boyle, E.I., et al., *GO::TermFinder--open source software for accessing Gene Ontology information and finding significantly enriched Gene Ontology terms associated with a list of genes.* Bioinformatics, 2004. **20**(18): p. 3710-5.

36. Pirzgalska, R.M., et al., *Sympathetic neuron-associated macrophages contribute to obesity by importing and metabolizing norepinephrine.* Nat Med, 2017. **23**(11): p. 1309-1318.

37. Camell, C.D., et al., *Inflammasome-driven catecholamine catabolism in macrophages blunts lipolysis during ageing.* Nature, 2017. **550**(7674): p. 119-123.

38. Rogers, N.H., et al., *Aging leads to a programmed loss of brown adipocytes in murine subcutaneous white adipose tissue.* Aging Cell, 2012. **11**(6): p. 1074-83.

39. Sun, W., et al., *snRNA-seq reveals a subpopulation of adipocytes that regulates thermogenesis.* Nature, 2020. **587**(7832): p. 98-102.

40. Zingaretti, M.C., et al., *The presence of UCP1 demonstrates that metabolically active adipose tissue in the neck of adult humans truly represents brown adipose tissue.* FASEB J, 2009. **23**(9): p. 3113-20.

41. Tsagkaraki, E., et al., *CRISPR-enhanced human adipocyte browning as cell therapy for metabolic disease.* Nat Commun, 2021. **12**(1): p. 6931.

42. Wang, C.H., et al., *CRISPR-engineered human brown-like adipocytes prevent diet-induced obesity and ameliorate metabolic syndrome in mice.* Sci Transl Med, 2020. **12**(558).

43. Stanford, K.I., R.J. Middelbeek, and L.J. Goodyear, *Exercise Effects on White Adipose Tissue: Beiging and Metabolic Adaptations.* Diabetes, 2015. **64**(7): p. 2361-8.

44. Liu, X., et al., *Brown adipose tissue transplantation improves whole-body energy metabolism.* Cell Res, 2013. **23**(6): p. 851-4.

45. Corvera, S., *Cellular Heterogeneity in Adipose Tissues.* Annu Rev Physiol, 2021. **83**: p. 257-278.

46. Rondini, E.A. and J.G. Granneman, *Single cell approaches to address adipose tissue stromal cell heterogeneity.* Biochem J, 2020. **477**(3): p. 583-600.

47. Emont, M.P., et al., *A single cell atlas of human and mouse white adipose tissue.* bioRxiv, 2021: p. 2021.11.09.466968.

48. Lamalice, L., F. Le Boeuf, and J. Huot, *Endothelial cell migration during angiogenesis.* Circ Res, 2007. **100**(6): p. 782-94.

49. Gunda, B., et al., *COL4A2 mutation causing adult onset recurrent intracerebral hemorrhage and leukoencephalopathy.* J Neurol, 2014. **261**(3): p. 500-3.

50. Lekkas, D. and G.K. Paschos, *The circadian clock control of adipose tissue physiology and metabolism.* Auton Neurosci, 2019. **219**: p. 66-70.

51. Dankel, S.N., et al., *Weight cycling promotes fat gain and altered clock gene expression in adipose tissue in C57BL/6J mice.* Am J Physiol Endocrinol Metab, 2014. **306**(2): p. E210-24.

52. Otway, D.T., et al., *Rhythmic diurnal gene expression in human adipose tissue from individuals who are lean, overweight, and type 2 diabetic.* Diabetes, 2011. **60**(5): p. 1577-81.

53. Aggarwal, A., et al., *The Circadian Clock Regulates Adipogenesis by a Per3 Crosstalk Pathway to Klf15.* Cell Rep, 2017. **21**(9): p. 2367-2375.

54. Sotak, M., et al., *Peripheral circadian clocks are diversely affected by adrenalectomy.* Chronobiol Int, 2016. **33**(5): p. 520-9.

55. Yamamoto, T., et al., *Transcriptional oscillation of canonical clock genes in mouse peripheral tissues.* BMC Mol Biol, 2004. **5**: p. 18.

56. Froy, O. and M. Garaulet, *The Circadian Clock in White and Brown Adipose Tissue: Mechanistic, Endocrine, and Clinical Aspects.* Endocr Rev, 2018. **39**(3): p. 261-273.

57. Adlanmerini, M., et al., *Circadian lipid synthesis in brown fat maintains murine body temperature during chronic cold.* Proc Natl Acad Sci U S A, 2019. **116**(37): p. 18691-18699.

58. Fernandez, N., et al., *Mouse Mesenchymal Progenitor Cells Expressing Adipogenic and Osteogenic Transcription Factors Suppress the Macrophage Inflammatory Response.* Stem Cells Int, 2017. **2017**: p. 5846257.

59. Kaplan, J.L., et al., *Adipocyte progenitor cells initiate monocyte chemoattractant protein-1-mediated macrophage accumulation in visceral adipose tissue.* Mol Metab, 2015. **4**(11): p. 779-94.

60. Gealekman, O., et al., *Control of adipose tissue expandability in response to high fat diet by the insulin-like growth factor-binding protein-4.* J Biol Chem, 2014. **289**(26): p. 18327-38.

61. Guo, D.H., et al., *Beige adipocytes mediate the neuroprotective and anti-inflammatory effects of subcutaneous fat in obese mice.* Nat Commun, 2021. **12**(1): p. 4623.

62. Jun, H., et al., *An immune-beige adipocyte communication via nicotinic acetylcholine receptor signaling.* Nat Med, 2018. **24**(6): p. 814-822.

63. Bour, S., et al., *Adipogenesis-related increase of semicarbazide-sensitive amine oxidase and monoamine oxidase in human adipocytes.* Biochimie, 2007. **89**(8): p. 916-25.

64. Sturza, A., et al., *Monoamine oxidase is a source of oxidative stress in obese patients with chronic inflammation (1).* Can J Physiol Pharmacol, 2019. **97**(9): p. 844-849.

65. Garcia-Alonso, V., et al., *Prostaglandin E2 Exerts Multiple Regulatory Actions on Human Obese Adipose Tissue Remodeling, Inflammation, Adaptive Thermogenesis and Lipolysis.* PLoS One, 2016. **11**(4): p. e0153751.

66. Lim, J., et al., *Depot-specific UCP1 expression in human white adipose tissue and its association with obesity-related markers.* Int J Obes (Lond), 2020. **44**(3): p. 697-706.

67. Yu, J., et al., *MiR-27b-3p Regulation in Browning of Human Visceral Adipose Related to Central Obesity.* Obesity (Silver Spring), 2018. **26**(2): p. 387-396.

68. Mabbott, N.A., et al., *An expression atlas of human primary cells: inference of gene function from coexpression networks.* BMC Genomics, 2013. **14**: p. 632.

FIGURE 1

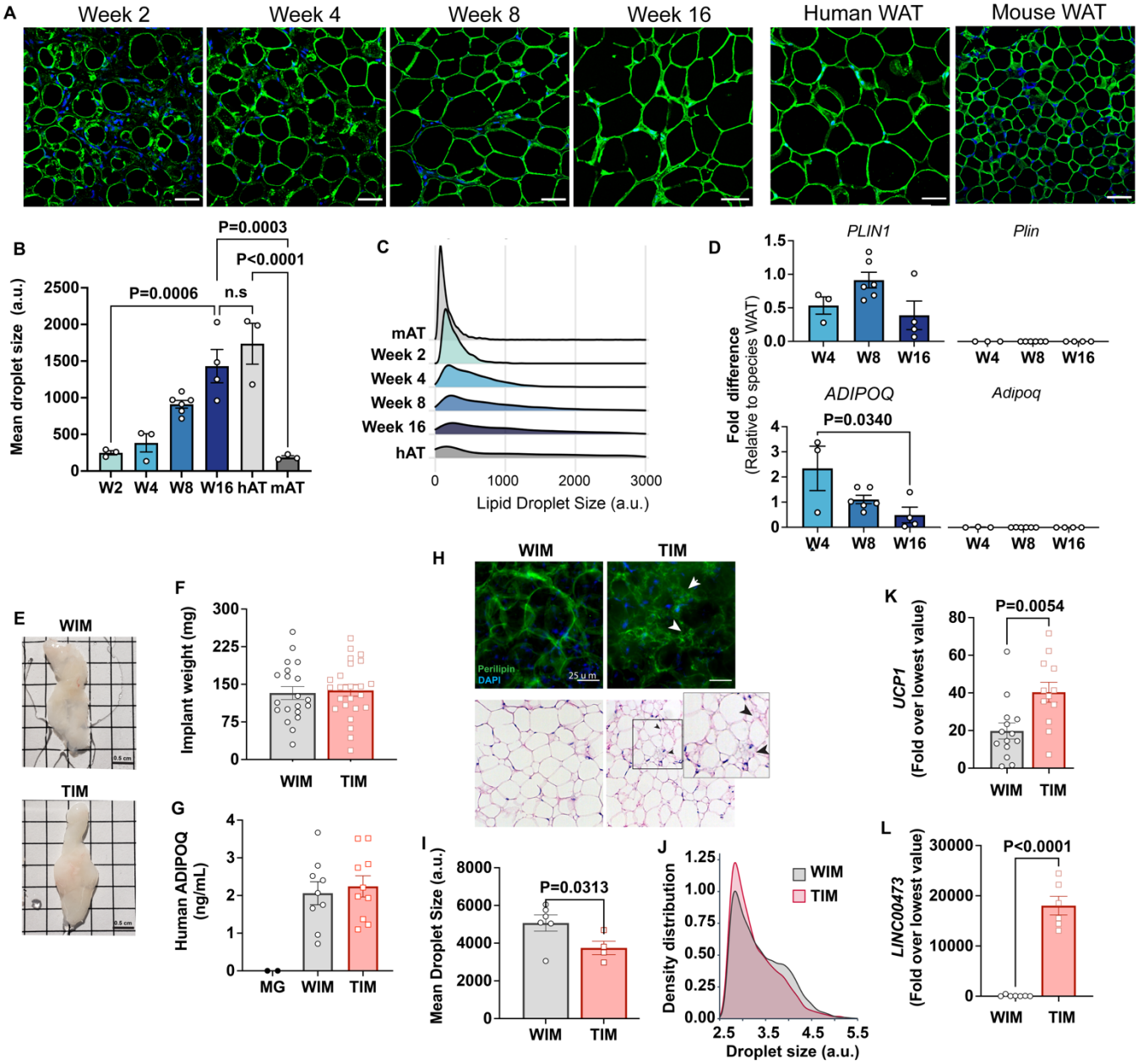

Figure 1. Characteristics of adipocytes during development of WIM and TIM. A. Representative images of PLIN1 (green) and DAPI (blue) staining of WIM at the indicated weeks after implantation, and of inguinal mouse and subcutaneous human adipose tissue, scale bar = 50 µm. **B.** Quantification of droplet size of PLIN1-stained implants and tissues. Each symbol represents the mean area of all cells within three random fields of a single implant or tissue section. Bars represent the means and SEM of n=3 n=3, n=6, n=4, implants at weeks 2, 4, 8 and 16 respectively, and n=3 for independent human or mouse adipose tissue

samples. Statistical significance of the differences between samples was calculated using one-way ANOVA with Tukey's adjustment for multiple comparisons, and exact P-values are shown. **C.** Density distribution plot of droplet size of developing implants and control tissue. Each density distribution represents the combined density of all samples for each group (n = 3-6). **D.** RT-PCR of excised implants using species-specific probes for genes indicated. Values were normalized to those obtained from human or mouse adipose tissue samples exemplified in A. Symbols are the means of technical duplicates for each implant, and bars are the means and SEM of n=3, n=6 and n=4 implants at weeks 4, 8 and 16 respectively. Statistical significance of the differences between samples was calculated using one-way ANOVA with Tukey's adjustment for multiple comparisons, and exact P-values are shown. **E.** Representative images of white implants (WIM) and thermogenic implants (TIM) at 8 weeks of development, grid size = 0.5 cm. **F.** Weight in mg of each excised implant from bi-laterally implanted mice. Bars are the mean and SEM of n=20 and n=24 implants for WIM and TIM, respectively. **G.** Circulating human-specific adiponectin (ng/ml) from bilaterally-implanted mice. Symbols are the mean of technical duplicates for n=2, n=9 and n=10 mice implanted with Matrigel alone (MG), WIM or TIM respectively. **H.** Whole mounts of WIM and TIM at 8-weeks after implantation stained for PLIN1 (top panels), or with H&E. Arrowheads highlight clusters of dense, multilocular droplets in TIM. **I.** Mean droplet size (arbitrary units) in WIM and TIM. Symbol represent the mean areas of all cells from two independent sections from each implant. Bars represent the mean and SEM of n=6 and n=4 WIM and TIM implants, respectively. Statistical significance of the difference was calculated using unpaired, one-tailed Student t-test and resulting P-value is shown. **J.** Density distribution plot of droplet size of WIM and TIM. Each density distribution represents the average density of all samples for each group. **K,L.** RT-PCR of excised implants using human-specific probes for the genes indicated. Symbols are the means of technical duplicates for each implant, and bars are the means and SEM of n=14 and n=12 for *UCP1*, and n=7 and n=6 for *LINC00473,* in WIM and TIM, respectively. Values were normalized to the lowest expression level in the entire data set of n=26 implants. Statistical significance of the differences was calculated using unpaired, two-tailed Student t-tests, and exact P-values are shown.

FIGURE 2

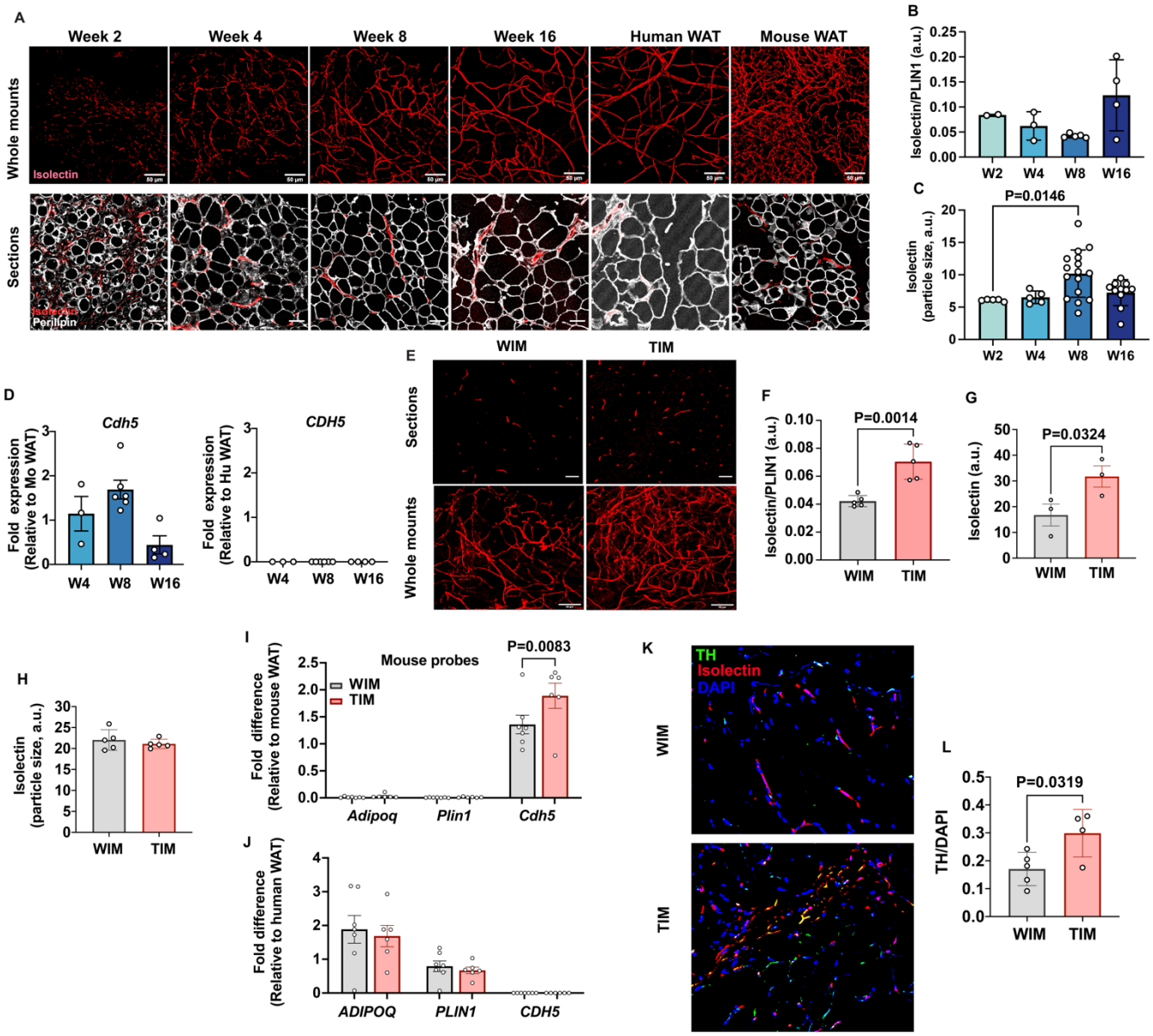

Figure 2. Vascular development of WIM and TIM. A. Representative images of isolectin staining of WIM at the indicated weeks after implantation, and of inguinal mouse and subcutaneous human adipose tissue, scale bar = 50 µm. **B.** Total isolectin staining in implants. Each symbol represents the sum of the areas of particles stained by isolectin, normalized to the total area stained by Plin1, of three random fields from a single implant. Bars represent the means and SEM of n=2, n=3, n=5, n=4, implants at weeks 2, 4, 8 and 16 respectively. C. Mean size of isolectin-stained particles. Each symbol represents the mean area of

particles stained by isolectin in three random fields per implant. Bars represent the means and SEM of n=5, n=5, n=16, n=11, implants at weeks 2, 4, 8 and 16 respectively. Significance of the differences between samples was calculated using one-way ANOVA with Tukey's adjustment for multiple comparisons, and exact P-values are shown. **D.** RT-PCR of excised implants using species-specific probes for *CDH5*/*Cdh5*. Values were normalized to those obtained from mouse adipose tissue samples. Symbols are the means of technical duplicates for each implant, and bars are the means and SEM of n=3, n=6 and n=4 implants at weeks 4, 8 and 16 respectively. **E.** Representative images of thin sections (upper panels) and whole mounts (lower panels) of WIM and TIM after 8 weeks of implantation, stained with isolectin. **F,G**. Total isolectin staining of thin sections and whole mounts, assessed as in (B). Bars represent the means and SEM of n=5, implants for thin sections, and n=3 for whole mounts of WIM and IM, respectively. Significance of the differences between samples was calculated using unpaired two-tailed Student t-tests. **H.** Mean size of isolectin-stained particles in WIM and TIM, analyzed as in (C). Bars represent the means and SEM of n=5, implants. **I,J.** RT-PCR of excised implants using mouse-specific (I) and human-specific (J) probes for the genes indicated. Values were normalized to those obtained from mouse and human adipose tissue samples. Symbols are the means of technical duplicates for each implant, and bars are the means and SEM of n=7, and n=6 WIN and TIM implants respectively. Significance of the differences between WIM and TIM for each gene was calculated using one-way ANOVA with the Holm-Sidak adjustment for multiple comparisons, and exact P-values are shown. **K.** Representative images of thin sections WIM and TIM after 8 weeks of implantation, stained for isolectin (red), tyrosine hydroxylase (TH, green) and DAPI (blue). **L**. Total TH staining, where bars represent the means and SEM of n=5, and n=4 sections of WIM and TIM, respectively. Significance of the differences between samples was calculated using un-paired 2-tailed Student t-test and the exact P-value is shown.

FIGURE 3

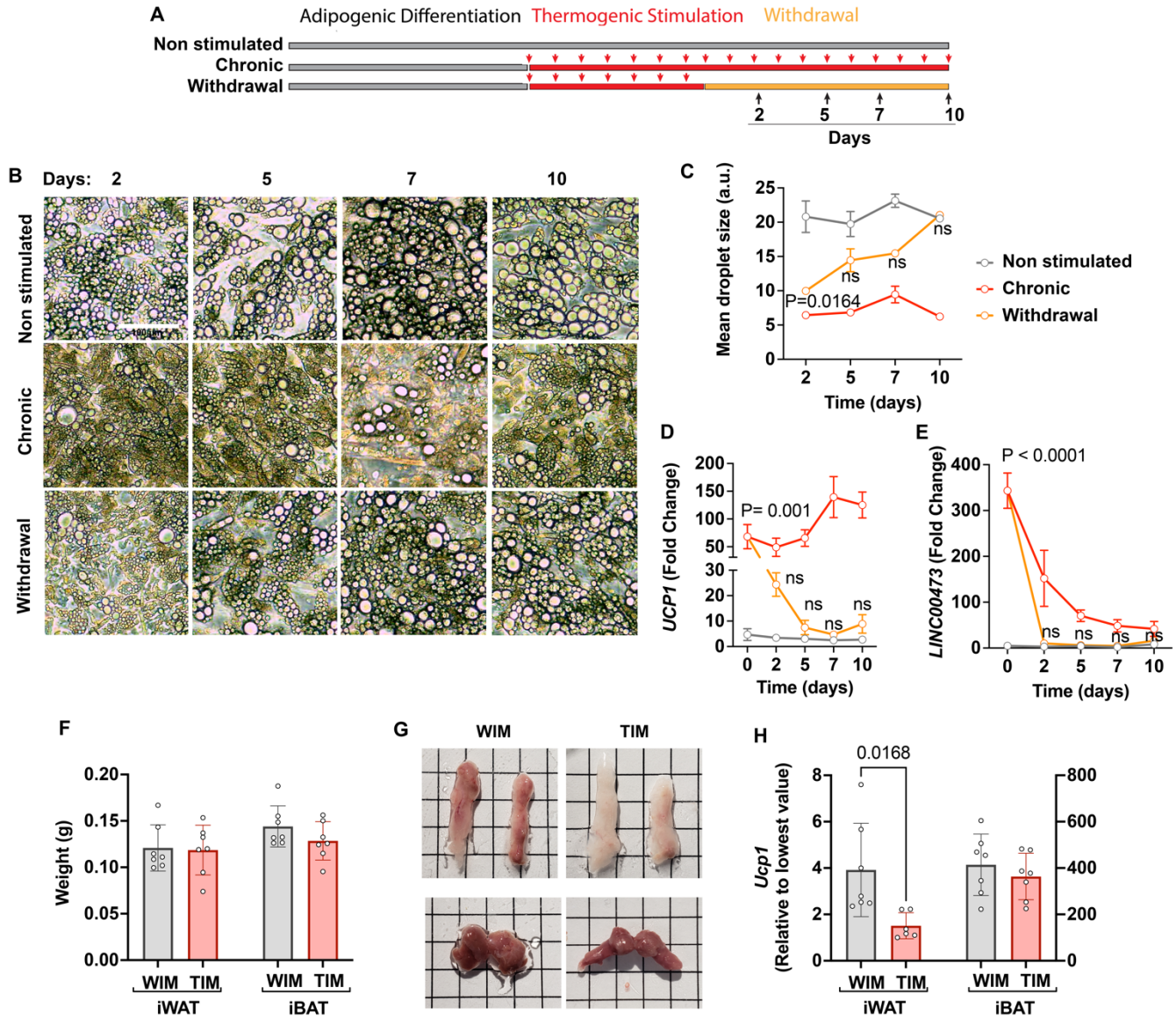

Figure 3. Capacity of thermogenic adipocytes to autonomously maintain their phenotype, and their effect on host adipose depots. A. Experimental paradigm for in vitro experiments. **B**. Phase images of cultured adipocytes during chronic stimulation and withdrawal. **C.** Quantification of droplet size, where symbols are the mean and SEM of all droplets in single images from each of n=3 independent culture wells. **D,E.** RT-PCR with human-specific probes for UCP1 (D) and LINC00473 (E), where symbols are the mean and error bars the SEM of n=3 independent culture wells assayed in technical duplicate. Values are

expressed as the fold difference relative to the lowest value in the dataset. For (C),(D) and (E), statistical significance of differences at each time point between the withdrawal and the non-induced group, was measured using 2-way ANOVA with Dunnet's multiple comparison test, and exact P-values are shown. **F.** Weight of excised inguinal (iWAT) and interscapular (iBAT) after 8 weeks of implantation with WIM or TIM. Symbols correspond to the summed weight of two inguinal or the single interscapular pad per mouse, and bars the mean and SEM of n=7 mice. **G.** Representative images of excised fat pads. Top panels, iWAT; bottom panels iBAT. **H.** RT-PCR of *Ucp1*, where each symbol is the mean of technical duplicates, and bars represent the mean and SEM of n=6-7 pads. Data are expressed as the fold difference relative to the lowest value in the set, with scales for iWAT and iBAT on the left and right Y axes, respectively. Statistical significance of differences was measured using non-paired, 2-tailed Student t-tests and exact P-values are shown.

FIGURE 4

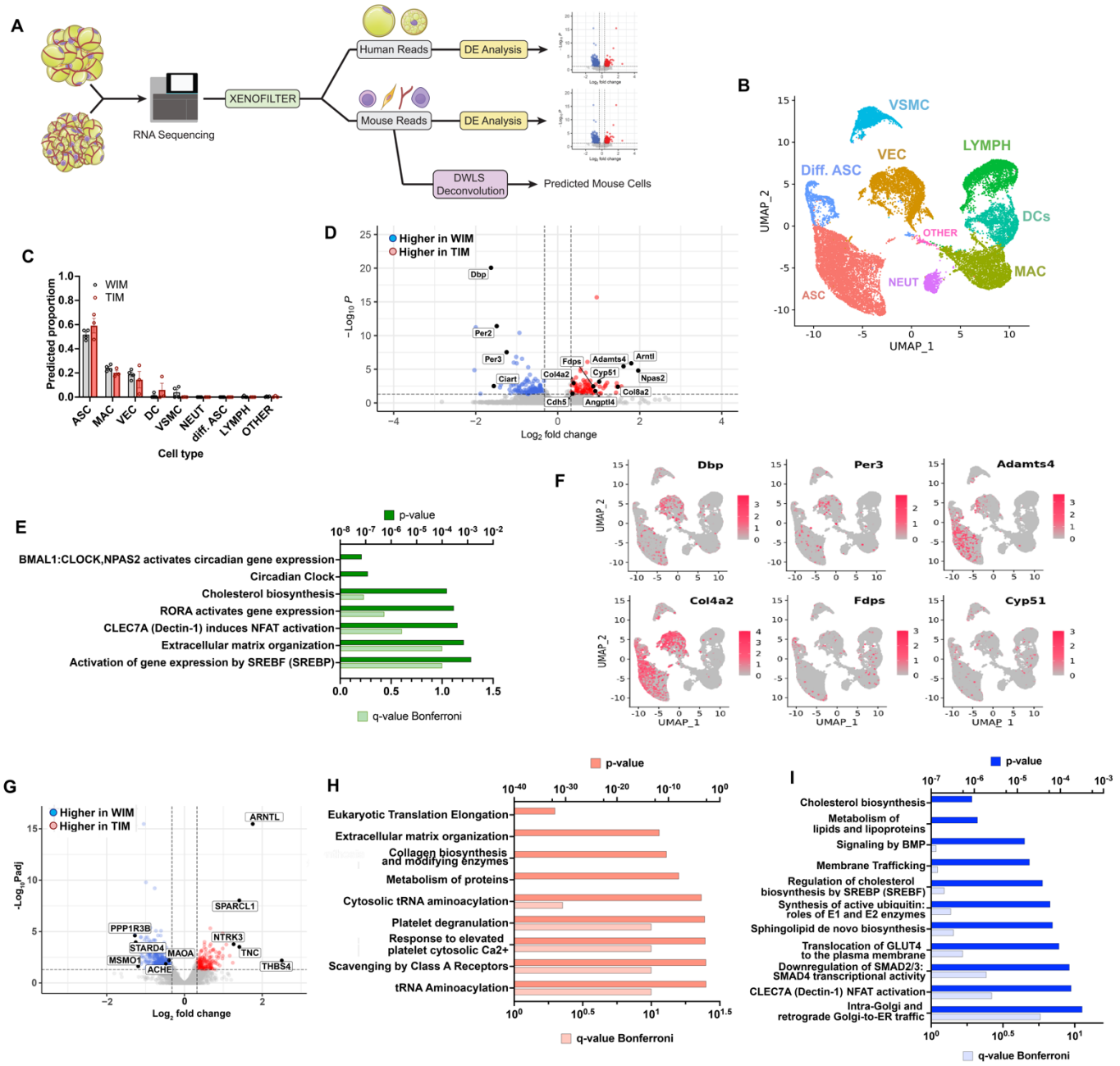

Figure 4. Distinct gene expression signtures of adipocytes and stromal cells in WIM and TIM. A. Overview of analysis paradigm. **B.** Dimensional reduction plot of data from Burl et al. [28], using Uniform Manifold Approximation and Projection (UMAP), where ASC = adipose stem cells, Diff. ASC = differentiating adipose stem cells, VEC = vascular endothelial cells, VSMC = Vascular smooth muscle cells, LYMPH = Lymphocytes, DCs = Dendritic cells, MAC = macrophages, NEUT = Neutrophils, OTHER = unidentified cluster. **C.** Predicted proportion of cells present in WIM and TIM. Symbols correspond to

data from an individual implant, and bars the mean and SEM of n=4 and n=3 WIM and TIM respectively. **D.** Volcano plot of genes mapping to the mouse genome which are differentially expressed between WIM and TIM. **E.** Pathway (REACTOME) enrichment analysis of mouse genes differentially expressed between WIM and TIM. **F.** Mouse genes differentially expressed between WIM and TIM mapped onto the UMAP representation shown in (A), with cells expressing the indicated genes highlighted in red. **G.** Volcano plot of genes mapping to the human genome differentially expressed between WIM and TIM. **H,I.** Pathway (REACTOME) enrichment analyses of human genes more highly expressed in TIM (H) or WIM (I).

FIGURE 5

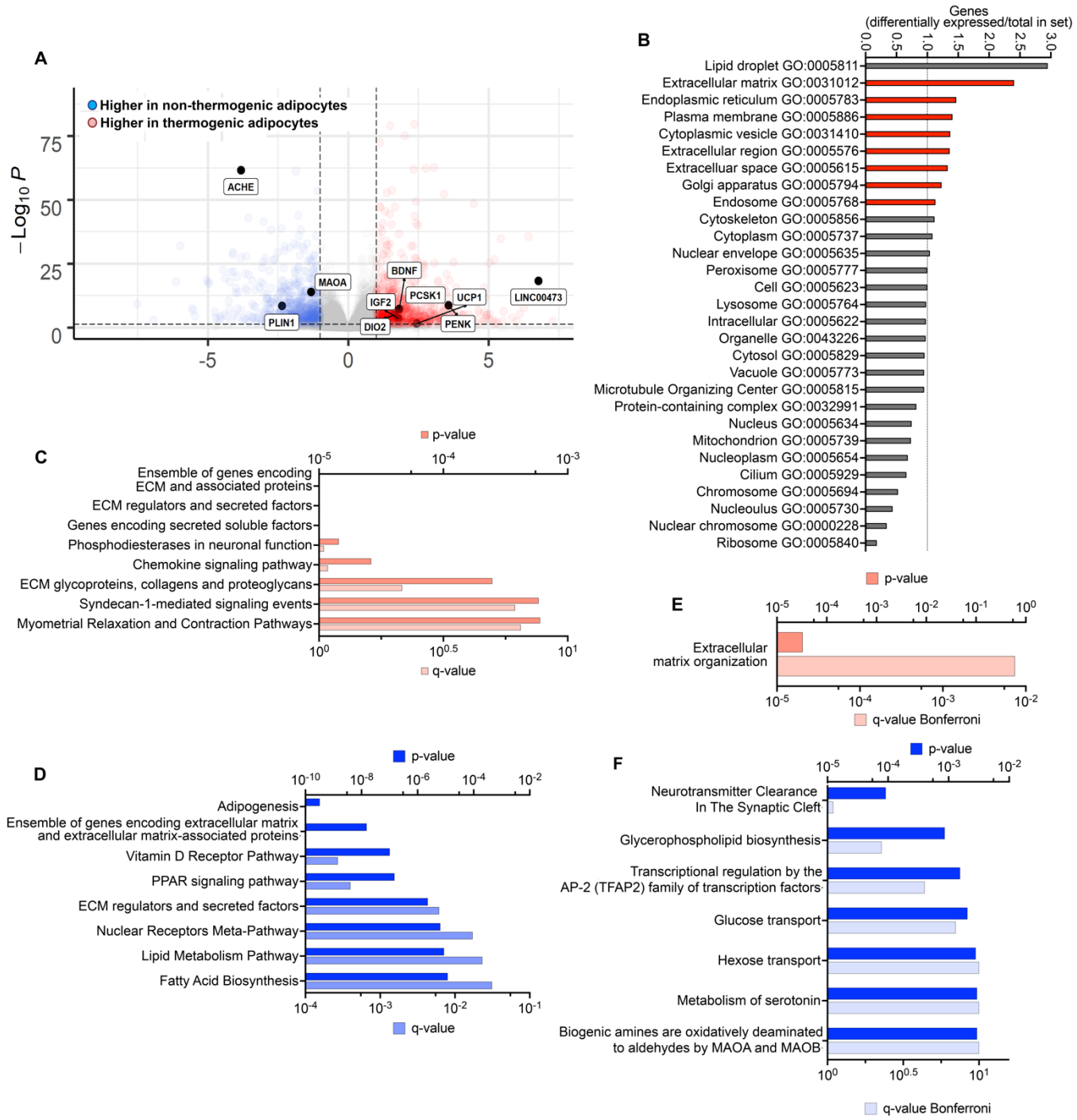

Figure 5. Differentially expressed genes persisting through tissue development. A. Volcano plot of genes differentially expressed between non-thermogenic and thermogenic adipocytes prior to implantation.

Highlighted are selected genes characterstic of human thermognic adipocytes and genes involved in the control of neurotranmission. **B.** Enrichment of GO categories by genes differentially expressed between non-thermogenic and thermogenic adipocytes, with categories for secretory proteins highlighted in red. **C,D.** Pathway (REACTOME) enrichment analyses of genes more highly expressed in thermogenic (C) or non-thermogenic (D) adipocytes. **E.** Pathway analysis of genes more highly expressed in thermogenic adipocytes that remained more highly expressed in TIM. **F.** Pathway analysis of genes more highly expressed in non-thermogenic adipocytes that remained more highly expressed in WIM.

FIGURE 6

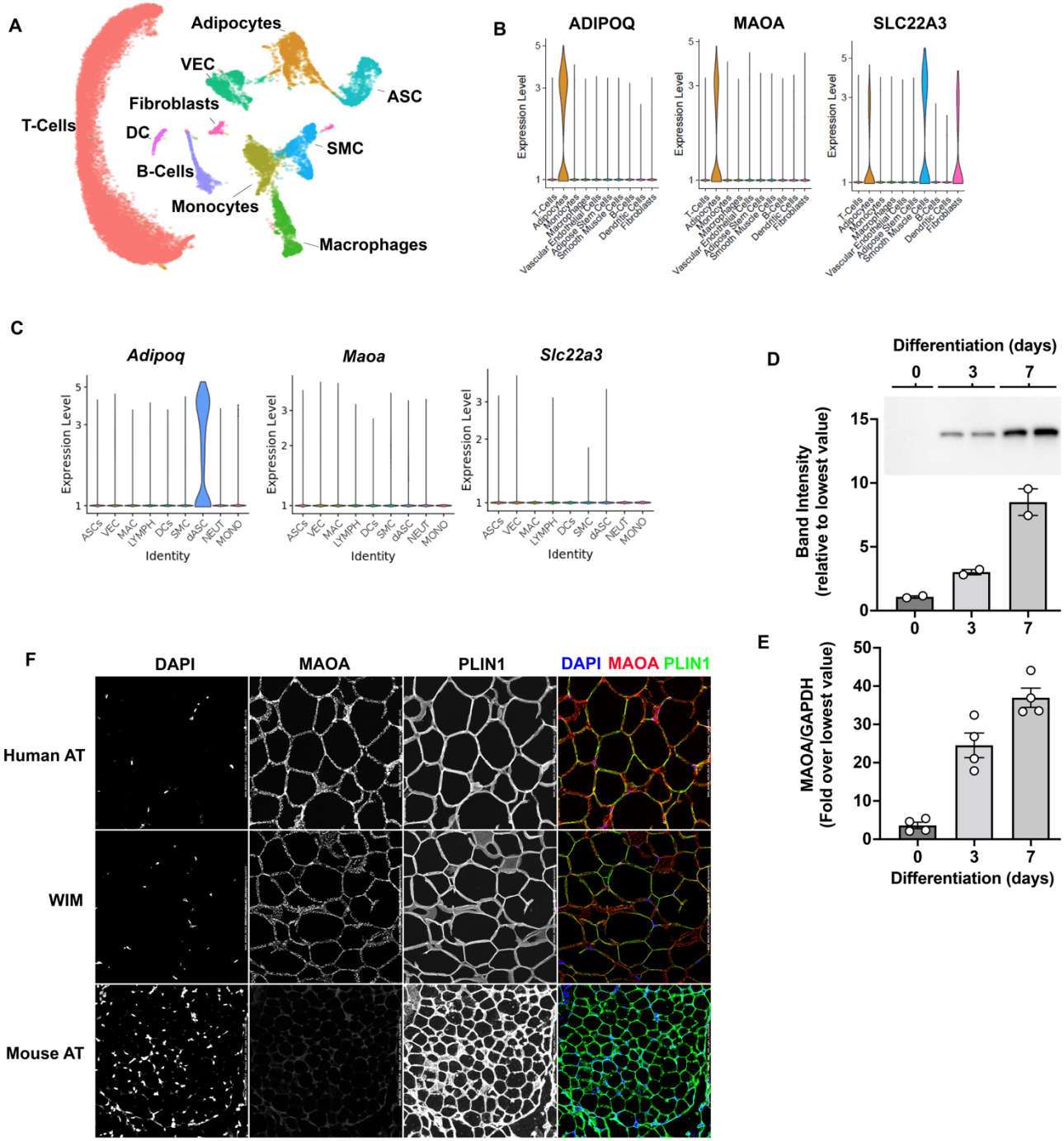

Figure 6. Species specific expression of MAOA in adipocytes. A. Dimensional reduction plot of data from Sun et. al. [39], using Uniform Manifold Approximation and Projection (UMAP). **B,C.** Violin plots

of indicated human and mouse genes from single cell data from Sun et. al. [39] (B) and Burl et al. [28] (C). **D.** Expression of MAOA at indicated days following induction of differentiation in human adipocytes. Samples were prepared from 2 independent wells and subjected to western blotting with an antibody to MAOA. The intensity of the single detected band was quantified and values plotted. **E.** RT-PCR for MAOA at indicated days following induction of differentiation in human adipocytes. Symbols represent the fold difference over the lowest value in the dataset, and bars the mean and SEM of n=4 independent cultures. F. Representative images of human subcutaneous adipose tissue, WIM, and mouse inguinal adipose tissue stained with antibodies to MAOA and PLIN1, and counterstained with DAPI. Similar results have been obtained with different antibodies reactive to mouse, human or both species.

EXTENDED FIGURE 1

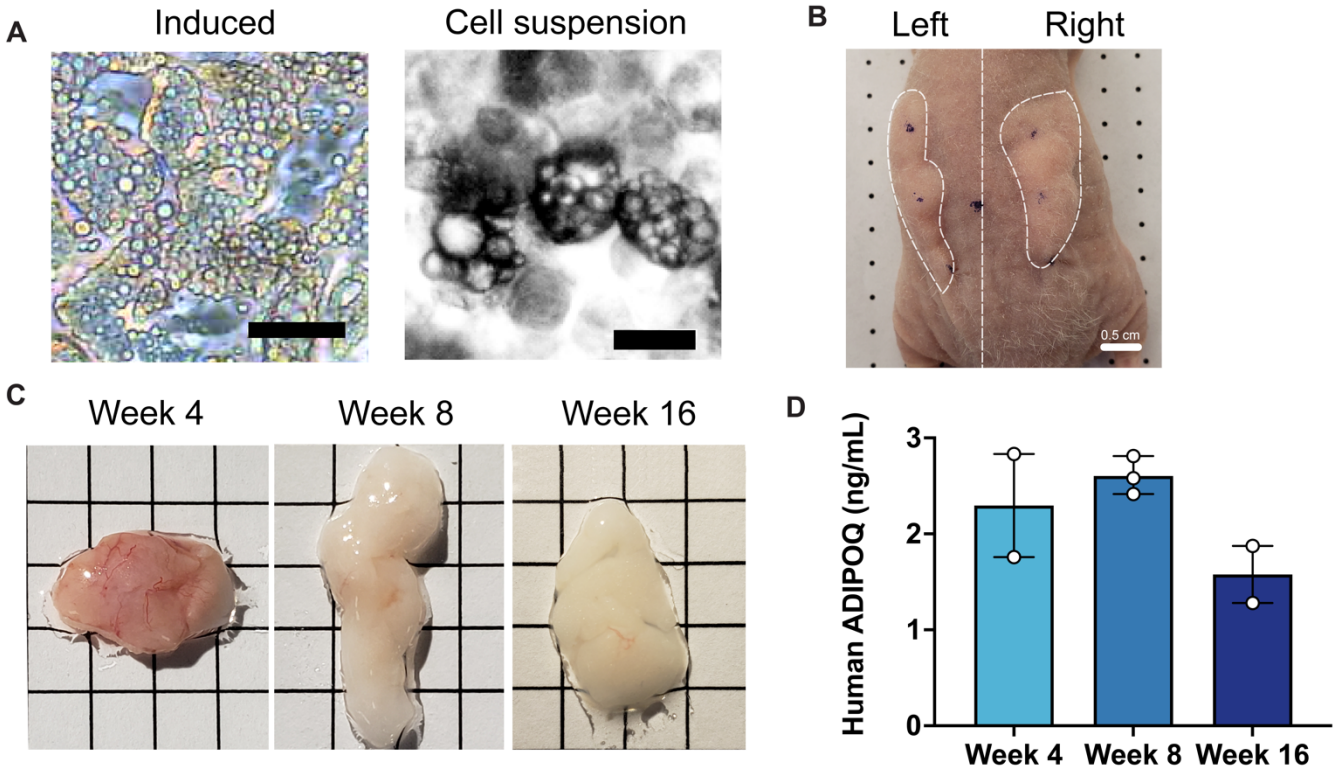

Extended Figure 1. Development of implants from cultured adipocytes in mice. A. Representative images of differentiated adipocytes and single cell suspension used for implantation, scale bar = 25 µm. **B.** Representative image of bilateral flank implantation, scalebar = 0.5 cm. **C.** Excised implants at 4, 8, and 16 weeks of development, grid size = 0.5 cm. **D.** Circulating human adiponectin at indicated weeks after implantation. Symbols represent the mean of technical duplicates for each individual mouse, bars represent the mean and range of n=2, n=3 and n=2 mice for weeks 4, 8 and 16 respectively.

EXTENDED FIGURE 2

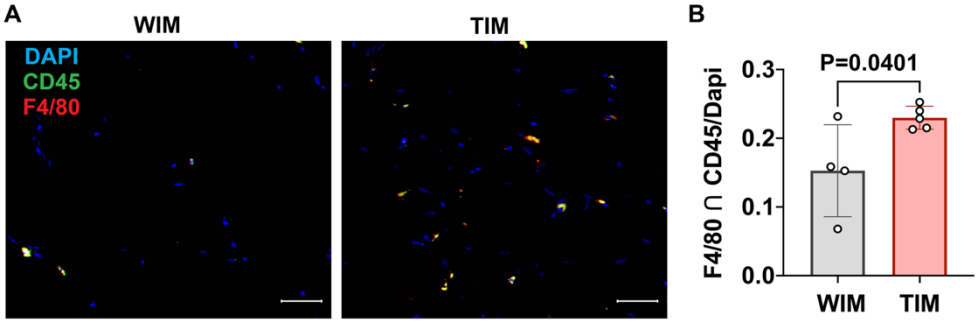

Extended Figure 2. Density of macrophages in WIM and TIM. A. Representative images of thin sections WIM and TIM after 8 weeks of implantation, stained for F4/80 (red), CD45 (green) and DAPI (blue). **B**. Macrophage staining, where symbols are the mean of three independent sections per implant, and bars represent the means and SEM of n=4 and n=5, WIM and TIM implants, respectively. Data represents the cells stained with both CD45 and F4/80, normalized to DAPI to account for section size. Significance of the differences was calculated using un-paired 2-tailed Student t-test and the exact P-value is shown.

TABLES

TABLE 1: Differential expression of mouse genes between WIM and TIM

Mouse genes higher in TIM			Mouse genes, higher in WIM		
ID	Fold difference relatve to WIM	padj	ID	Fold difference relative to TIM	padj
Gm2423	414.0165944	5.84E-15	Hlf	4.07490842	4.91E-05
Pck1	6.197534692	0.038521986	mt-Atp8	3.988527647	1.25E-11
Npas2	3.904671521	9.39E-05	Gt(ROSA)26Sor	3.083976138	0.038783497
Arntl	3.471334273	7.36E-06	Dbp	3.079314164	1.28E-20
Adamts4	3.047382949	1.93E-05	Ciart	2.930285259	0.008131954
Fmod	2.938451825	0.008161356	Per2	2.797251524	1.22E-11
Col8a2	2.768419924	0.009211934	Gm28438	2.749405893	3.99E-25
Diras2	2.717206346	0.002369715	Omd	2.646610704	0.010508996
Tenm4	2.709801632	0.008161356	Carnmt1	2.606562742	0.004201864
Prnd	2.547882498	2.05028E-04	Per3	2.365264244	4.99E-08
Thbs4	2.309613781	0.001753814	Klf5	2.19519001	0.005804325
Has3	2.255648091	0.004671439	Gpr165	2.111174655	0.004348326
Hmcn1	2.232601242	0.007202355	Lonrf1	2.101253793	0.036598722
Cyp26b1	2.166381404	0.011863103	Fmo2	2.09962451	5.24995E-04
Nfil3	2.040436341	0.006811439	Tef	2.095069684	7.92E-07
Cyp51	2.021405639	0.001384968	Doc2b	2.065456324	0.021063734
Rflnb	1.93710492	6.33E-18	Cys1	2.033892565	0.003760753
Pcdh12	1.90524311	0.003343828	Flrt2	2.01711208	0.015687874
Angptl4	1.890697785	0.023923376	Pik3ip1	2.012963136	1.61E-07
Fdps	1.828309259	0.005990864	Nr1d2	1.994990621	1.76E-06
Rasl11b	1.75543197	0.008161356	Kcnt1	1.983886547	0.02426168
Bcl3	1.752166864	0.015719401	Wee1	1.97232078	3.65727E-04
Ccl24	1.745082205	0.015464088	Nrn1	1.953226507	0.025767854
Bcar3	1.742170045	0.019392531	Gm10053	1.936944639	0.03118318
Aqp7	1.739282361	5.43575E-04	Ccr1	1.920342764	0.008862338
Rasgrp3	1.708889218	0.022153188	mt-Nd2	1.913399412	0.005761879
Parm1	1.707558544	0.003104442	Gm10925	1.907892041	3.36E-05

Smpd3	1.69470215	0.016079957	Lyve1	1.906087314	1.62E-11
Cd83	1.685911995	0.002299406	Inmt	1.874754199	0.018920757
Tspan18	1.683551022	0.01113439	Sh3bgrl	1.871342886	0.020789825
Gm6166	1.676590317	0.02925211	Gm28661	1.868249746	6.54E-05
Aoc3	1.667334391	0.008161356	mt-Nd4	1.824473054	0.001726744
Unc5b	1.659148877	0.003104442	Galnt15	1.821907266	1.33E-07
Eln	1.655545145	4.30E-07	Fam107a	1.820357381	0.038521986
Sytl2	1.645801763	5.34702E-04	Fzd1	1.806827454	0.002707857
Gm8203	1.623862341	0.039559482	F630028O10Rik	1.793756857	0.038521986
Leo1	1.612144807	0.039181712	Etv1	1.76112702	0.045558332
Errfi1	1.60973201	0.001223419	Zkscan8	1.749121582	0.01995958
Akap12	1.60800538	2.96E-05	Pde7b	1.743213268	0.001423749
Apln	1.60572157	0.01121383	Trp53inp1	1.731604407	0.038962943
Bmp6	1.602485018	0.048860886	Acss3	1.712346715	0.004073625
Efr3b	1.586478987	0.008161356	Vegfd	1.701189111	5.43575E-04
Arrdc4	1.576196154	0.001812823	Tmem47	1.700074521	0.022153188
Fst	1.576013515	8.84948E-04	mt-Rnr2	1.687922885	7.35E-07
Prr5	1.567527103	0.014432361	Spred1	1.679934141	0.045762614
Hba-a1	1.565149612	0.019398331	Ppl	1.676262961	2.28790E-04
Col5a3	1.547258944	3.08812E-04	Ackr2	1.67150869	0.045558332
Mvk	1.540600064	0.039554103	Gpcpd1	1.653479272	4.97783E-04
Cyth1	1.532415479	0.0182558	Pgk1	1.648677473	0.037402729
Myh11	1.530007286	0.016964706	Ogfrl1	1.643189581	4.12E-06
Lss	1.51172549	0.045558332	Lepr	1.636919769	0.037218164
Tmem132a	1.50274977	0.03576063	mt-Nd1	1.630227686	0.021063734
Nes	1.492860175	0.048860886	Calcrl	1.623831791	0.001223419
Jup	1.480195476	1.76E-06	Cited2	1.617472599	0.012484889
Gprc5c	1.473514823	6.77E-06	Fcho2	1.608635792	0.009211934
Rin3	1.46494523	0.004387827	Ms4a4a	1.596840113	7.22E-05
P2ry6	1.461732858	0.001410202	Map3k6	1.595435924	0.023146246
Gadd45g	1.453435852	0.009211934	Gm28437	1.585430769	0.008131954
Sh3pxd2b	1.446883799	0.038533759	Coq10b	1.577261367	0.046698433

Pprc1	1.411358287	0.021835662	Nr1d1	1.566009789	0.006679902
Ccnd2	1.403701891	0.048517392	Mpp5	1.563861595	0.017111068
Lrrc8d	1.398374853	0.005990864	Tlr13	1.552399466	0.01937081
Myd88	1.386897017	0.009939426	Irs2	1.536335443	0.015777396
Tuba1c	1.384464042	0.017111068	Rap2c	1.533555256	0.038521986
Map3k11	1.377495068	0.005990864	Man2a1	1.529614278	0.001516656
Daam2	1.372793336	0.037797296	Dmd	1.528869349	0.018264218
Septin4	1.365081283	0.001384968	Arrdc3	1.523959857	0.010879112
Slco2a1	1.363373397	0.011872025	Fzd7	1.523642664	0.021527147
Tmem252	1.351898494	0.048182691	Ubald2	1.514535402	0.005069359
Plxnd1	1.350992236	0.001877932	Abcb7	1.513536735	0.038521986
Ccnd1	1.348833514	5.34702E-04	Ube3a	1.50331188	0.037784656
Cnn2	1.340320485	0.032340219	Lysmd2	1.496684914	0.037402729
Zbtb7b	1.317985314	0.048860886	Ppp3cb	1.494801946	4.04151E-04
Col4a2	1.309805469	2.28790E-04	Serp1	1.491275407	0.016963072
Tgfb1	1.308420327	0.045762614	Lnpep	1.485785763	0.045762614
Col4a1	1.296906393	3.62E-05	Pcmtd2	1.477538955	0.037784656
Elmo2	1.288290139	0.0472543	Ptp4a1	1.470184332	0.008862338
Cdh5	1.287584127	0.031856915	Rora	1.468937005	0.0254307
B4galt5	1.286740167	0.037850408	Rhobtb3	1.467868955	0.048860886
Nid2	1.281730623	0.0472543	Tspan4	1.466062986	0.007870817
Itpkb	1.271718002	6.25098E-04	Gstt2	1.462959491	0.01121383
Lgals1	1.270656817	0.017232927	Cry2	1.459353428	0.015316403
Vcl	1.268338287	0.034179565	Ppp1cb	1.454973741	0.020145252
Zfp592	1.266065312	0.029946419	Ube2d3	1.446332163	0.032069321
Itga1	1.261313996	0.021527147	Ube2g1	1.443332189	0.009830218
Notch1	1.259939576	0.016963072	Rb1	1.439975929	0.045558332
			Lypla1	1.43722938	0.011917947
			Cpeb1	1.431775777	0.027989136
			Msr1	1.431345925	0.032714767
			Abcg2	1.426751478	0.025817324
			Osr1	1.422902731	0.018338339
			Gm4332	1.418725323	0.017836482
			Nfxl1	1.417216232	0.039554103

Casp4	1.402269147	0.042568826
Cyp4b1	1.399761275	4.04151E-04
Ms4a6d	1.397353673	0.007144453
Zfand5	1.390062945	0.012210612
Pcgf5	1.389640166	0.048860886
Mt2	1.387330301	0.017836482
Celf2	1.366544706	0.049987897
Arl5a	1.361160841	0.029421463
Dram2	1.357142712	0.035895444
Casp12	1.355834197	0.006873026
Vmp1	1.348755768	0.002347799
Adgrl4	1.347373658	0.0472543
Rin2	1.343773654	0.015483774
Xdh	1.343262034	0.001753814
Arih1	1.34111841	0.001250716
Fam76a	1.337056489	0.020517022
Dock9	1.335629994	0.001812823
Pcmtd1	1.333960688	0.005990864
Ddx3y	1.329140099	0.01995958
Ppp3ca	1.328953517	0.021527147
Ube2q2	1.324932252	0.020679261
Sypl	1.314889346	0.012484889
Mrtfb	1.308559483	0.007010349
Ppp3r1	1.305123004	0.007812406
Selenot	1.288611653	0.045762614
Arid5b	1.285597462	0.037784656
Osbpl11	1.281075095	0.039576459
Hook3	1.266528284	0.049043997
Ly6c1	1.258830979	4.25E-05
Anxa11	1.250889463	0.021170026
Ipo7	1.250351599	0.035895444

TABLE 2: Differential expression of human genes between WIM and TIM

Human genes higher in TIM

ID	Fold difference relative to WIM	padj
THBS4	5.672222027	0.006482511
ARNTL	3.378989219	3.40E-16
TNC	2.66109161	3.08041E-04
SPARCL1	2.659080912	9.32E-09
NTRK3	2.40373463	1.69715E-04
ELN	2.366500911	0.01092514
IFIT3	2.24089161	0.002232955
C1QTNF3	2.108281956	1.81718E-04
IFIT2	1.981146827	0.002273401
ZBTB16	1.976517492	4.50448E-04
CREB3L1	1.975588131	1.52E-05
MIR503HG	1.966883652	0.004201784
NES	1.874191899	0.020201792
BGN	1.865923752	0.0010618
DEPP1	1.853760426	0.001220209
PYCR1	1.846937112	0.002232955
DPT	1.825225176	0.003644521
TAGLN	1.80735874	0.014297669
FABP5P7	1.776102361	0.002718094
COL1A1	1.7523463	9.88674E-04
SEPTIN6	1.747177601	0.007404498
ADAM19	1.745455829	0.011854469
GDPD5	1.713259591	0.046490521
PRPH2	1.707514352	0.010127737
SLC7A8	1.679230321	5.29602E-04
CRABP2	1.666645072	6.21185E-04
SMOC2	1.658992907	0.006801323
RGS3	1.653108151	0.040033391
P3H3	1.652636127	6.21635E-04

Human genes higher in WIM

ID	Fold difference relative to TIM	padj
PPP1R3B	2.421548198	2.44E-05
LBHD1	2.41798496	1.52E-05
STARD4	2.385210173	1.09891E-04
PPL	2.376563504	3.85688E-04
MSMO1	2.282038734	0.023689262
SCOC	2.20474823	3.74329E-04
ID4	2.204439244	6.29777E-04
ABCA5	2.193510394	0.001057016
MBNL3	2.18442939	3.42E-06
SLC25A36	2.184268773	8.43E-06
HIGD1A	2.180430946	3.56E-05
ETFRF1	2.175831025	0.002641705
PER2	2.171174925	3.47E-05
ZBTB41	2.162196551	0.009757157
SLC35A3	2.162131655	0.014288719
SCAI	2.144107569	1.45179E-04
PHIP	2.126157964	0.001171324
CAMKK1	2.121293755	0.002288628
CYGB	2.102175711	7.56036E-04
ATG9B	2.09690771	7.28282E-04
DTWD1	2.089348904	0.003402445
UBE2W	2.080322185	8.35003E-04
MTRNR2L12	2.066732128	3.40E-16
HMGCR	2.042018389	7.82E-06
FOXN2	2.041420307	7.53490E-04
TMEM106B	2.038661416	6.81E-05
IER3IP1	2.031282729	0.008577315
SCAMP1	2.028369702	9.16663E-04
TMED7	2.015180865	0.002959317

CTHRC1	1.643042366	0.007791431
TNNT3	1.639170042	0.040929621
DDIT4	1.632960101	0.013444938
PCOLCE	1.617086507	0.002789157
RCOR2	1.616369799	0.034814803
MFAP2	1.615583713	0.029782754
AFF3	1.604218448	0.015269119
RHOBTB1	1.60419005	0.020910746
SNCG	1.603768082	0.010629699
FMOD	1.60172706	0.026055325
ANGPTL1	1.597374633	0.033522726
MMP14	1.59731144	1.65206E-04
CPXM1	1.594924975	0.038686211
NME1-NME2	1.589121379	0.030894038
FGD5	1.587844044	7.85400E-04
LSM7	1.587445854	0.035208519
TRIL	1.585185428	4.81E-06
ITGBL1	1.580500219	0.003129067
NFIL3	1.578550292	0.013722883
RCN3	1.577542585	0.00620459
HAVCR2	1.57313547	0.014297669
H19	1.5722143	2.53907E-04
CHST3	1.569166975	0.003208808
ID3	1.568839771	0.036530056
ZNF469	1.568649013	0.042222291
CDR2L	1.56049601	0.016887951
ZFP36	1.559687437	0.001171324
GADD45B	1.554414447	0.01073743
COL12A1	1.550291231	0.006482511
COL8A1	1.537955646	0.020306804
OAS1	1.527713543	0.047612016
IGF2	1.524986587	0.02812275
CILP	1.519843445	0.019850394
S1PR2	1.518198734	0.038900789

CYP4F22	2.001540995	0.034437929
ETNK1	1.99952651	0.006506961
CEPT1	1.99358956	3.97E-05
PER3	1.988375899	1.61E-10
GUF1	1.975612594	0.008808058
CASD1	1.971285198	0.00553322
RNF125	1.951117116	0.017186474
CPEB2	1.950432061	1.84969E-04
NUDT7	1.943864183	0.033432878
C1GALT1	1.940010176	1.01091E-04
HLF	1.939291404	3.54E-05
GNG10	1.936820177	1.65206E-04
TTLL7	1.933333148	0.001724906
UHMK1	1.925375731	3.74329E-04
SLC16A7	1.919440619	0.001724906
ACVR1C	1.919217019	0.01092514
ZNF117	1.916150909	7.53490E-04
C2orf69	1.905615572	3.63949E-04
FAM126B	1.903858143	0.009346922
EDNRB	1.901025076	0.021338695
LRRC8B	1.881175877	6.60E-05
ERI1	1.879445188	0.003644521
PTAR1	1.878165633	0.001242964
MTCO1P12	1.8780478	2.02E-06
SLC30A1	1.877721084	0.001556505
HEPN1	1.874340466	0.009314869
BMI1	1.871983305	0.002247298
LIN7C	1.870877477	0.018788117
MREG	1.859739879	0.003155279
RAB30	1.857156047	5.53707E-04
FAM199X	1.854217415	0.001242964
POLR2M	1.848927259	0.002959317
MINDY2	1.847100491	0.007132525
ANO3	1.843788882	6.66840E-04

GPX7	1.511133406	0.014830265
P3H4	1.499881983	0.026466925
SSC5D	1.498107518	0.007132525
JDP2	1.496221944	0.038900789
SBDSP1	1.495906562	0.046088337
ZBED3	1.493237254	0.009399688
SCARA3	1.485126185	0.005818969
NPAS2	1.483461166	0.002062245
RBM38	1.482923574	0.04543617
FKBP10	1.470483986	0.00806762
RPS28P7	1.463592107	0.014135585
STING1	1.463145837	0.044944421
TOB2	1.463013527	4.94046E-04
RPL12	1.460968238	9.75751E-04
FNDC5	1.460140035	0.035208519
COL1A2	1.459764687	0.025730834
DUSP7	1.459439926	0.03791988
IFIT1	1.458854696	0.033557682
DCHS1	1.456819518	0.024951235
LEP	1.456103084	0.04435373
POLR3H	1.452049834	0.025405348
DENND2A	1.450366736	0.009082288
PFDN6	1.446271144	0.036042847
FSCN1	1.443863224	0.04683534
SLC7A1	1.437669112	0.006070688
PKIG	1.429644784	1.03593E-04
NDEL1	1.426800885	1.78439E-04
ZNF740	1.425950284	0.001926863
PFKFB3	1.42492778	3.63949E-04
MRC2	1.424259665	0.004115189
NUPR1	1.423610558	0.009608812
SRGAP1	1.423522674	0.04073497
GAB2	1.421352054	0.003927729
ATP5IF1	1.420235178	0.00411518
ORAI2	1.419090059	0.047612016
ISLR	1.412597568	0.005568504

PANK3	1.833955407	1.18625E-04
TBL1XR1	1.833049203	0.001873654
SRP9	1.829852894	0.001556505
TMX3	1.829395089	4.29E-06
SGPP1	1.825958112	0.008417134
GCSH	1.823565958	0.001873541
SNX10	1.822928436	9.10613E-04
ZYG11B	1.822503686	9.49E-05
MICU3	1.811469625	0.019434033
GOLT1B	1.811151501	0.033183672
GLCCI1	1.797360413	8.35092E-04
FAM76A	1.792372019	6.64894E-04
ABHD13	1.787477639	0.046088337
DCUN1D1	1.774886433	0.003644521
GOLGA8N	1.77143829	5.72864E-04
DYNLT3	1.769819488	6.03256E-04
LRRC58	1.764813826	0.021612084
SH3BGRL	1.76073692	0.003861601
CRYZ	1.754484383	0.021990588
DRAM2	1.749819775	0.013493117
NTRK2	1.74564289	0.010281112
SLC25A46	1.744063914	0.002915779
PIGF	1.743359227	0.025853687
PER1	1.742193457	0.027638169
PIK3C2A	1.742045145	7.04759E-04
MIB1	1.741441769	0.011995199
LANCL1	1.739141786	6.81E-05
RICTOR	1.73666354	0.034814803
RORA	1.733683254	0.035628462
IL6ST	1.726579725	3.75145E-04
C5orf30	1.723837234	0.002226258
NXT2	1.716937036	0.020997421
ZMAT3	1.715958271	0.007360533
TNPO1	1.715592006	3.74329E-04
LATS1	1.714921029	0.003821449
ZDHHC21	1.712855385	0.039233809

ATP6V0E2	1.396370844	0.038409462
PMM2	1.396086108	0.032156001
C12orf57	1.39066118	0.021128156
ATF5	1.390460182	0.00747666
PTGIS	1.384593657	0.042638471
HCFC1R1	1.383261249	0.043124855
BTG2	1.38308796	0.003208808
ALDH1L2	1.378651976	0.008415925
ATF4	1.376596515	0.010219212
NID2	1.374858801	0.033001685
FLYWCH2	1.373289317	0.038620834
TIMP1	1.372717558	0.023754707
NDRG2	1.371831821	0.003208808
HEG1	1.370941798	0.033522726
APOL2	1.370282368	0.031619639
LHFPL2	1.370118629	0.027815151
COX7A1	1.369012559	0.012735835
ACVR1B	1.368951321	0.018338883
ARHGAP24	1.368768768	0.049453789
CCDC69	1.364833123	0.044558703
ADAMTS15	1.362110353	6.64894E-04
TCEAL4	1.358973641	0.044558703
P4HA2	1.357979283	0.015679215
MXRA5	1.3578481	0.01691395
FOSL2	1.357015566	0.005598489
PAPLN	1.352692074	0.031133611
GALNT10	1.350633937	0.006105685
TPM4	1.350183805	7.53490E-04
MYO1D	1.349761019	0.03360203
RPS11	1.342868035	9.04460E-04
TENM4	1.34057117	0.016942113
YARS1	1.339866533	0.020120461
RPL22P1	1.337763844	0.048420876
TARS1	1.337751334	0.006070688

GSKIP	1.71056505	0.017921592
TRIB1	1.707844675	6.81E-05
HSD17B12	1.70567181	0.001556505
RNF11	1.704650534	0.002232955
CD164	1.70247161	0.006889073
TSC22D3	1.699632585	6.13E-10
ZNF770	1.699342683	0.001261421
OIP5-AS1	1.69870962	0.001062976
GPR180	1.698001654	0.001926863
KITLG	1.695026514	0.024750919
VAMP4	1.694950819	0.010456752
SPCS3	1.694041243	0.024345671
MOB4	1.693468109	0.020997421
PTP4A1	1.692076407	0.01107548
LMO3	1.687910352	0.003833641
KATNBL1	1.687519134	0.001633295
SKIL	1.68354024	0.009347295
CALCRL	1.683085347	7.15E-05
HAND2-AS1	1.6784403	0.046687963
PTBP3	1.678247307	0.010650941
BMPR2	1.678014641	0.011792488
INO80D	1.67007815	0.004799367
LINC00899	1.666963107	0.011995199
POC1B	1.666816654	0.020997421
AKAP11	1.66508118	6.21185E-04
NR1D2	1.663382506	8.43E-06
MOB1B	1.658010359	0.0247612
OSTM1	1.657053285	0.001418004
LMBRD2	1.654353838	0.022693274
SYPL1	1.653699593	0.001926863
NHLRC3	1.652591229	0.001114082
EIF1AX	1.652561748	0.013722883
AP5M1	1.651425967	1.65650E-04
PCMTD1	1.651157972	0.001031618

SHMT2	1.337646096	0.031253256
CSTA	1.335741801	0.012093215
SARS1	1.334885577	0.009009353
ATP8B2	1.334221899	0.043133858
EIF5B	1.334083317	0.008432148
MED8	1.332549668	0.038900789
RPL38	1.332237024	0.006535645
COL3A1	1.331633565	0.031801669
PRDX4	1.327640875	0.033412431
MAP3K4	1.324869897	0.031128979
RAB7B	1.323931134	0.045894128
PRKRIP1	1.323891093	0.042903009
SDC3	1.323489981	0.012833953
SH3PXD2A	1.32252944	0.034392667
COL5A1	1.322121482	0.009347295
NFKBIA	1.321103107	0.020997421
TOMM7	1.321071597	0.004115189
ZFPL1	1.319634566	0.04380101
ERCC1	1.317924587	0.003307523
RPL28	1.316801572	0.035647619
ENC1	1.312362182	0.020910746
SLC29A1	1.31212422	0.004799367
COL6A1	1.309834803	0.014288719
ST3GAL4	1.309809177	0.024243247
CERCAM	1.30903261	0.004418702
MYH10	1.307070866	0.006889073
CTSZ	1.302845532	0.013760104
NUTF2	1.302665672	0.024250154
ADAMTS2	1.301546326	0.030570683
RPL18A	1.298495713	0.001705273
RPL8	1.296986247	0.008432148
TGFB3	1.296946764	0.041008453
GTPBP2	1.290739833	0.024250154
TMEM119	1.290377516	0.028032884
PPIB	1.290124871	0.033183672

C5orf24	1.651153325	0.016430447
LIMS1	1.650157995	9.04460E-04
RC3H1	1.648393378	0.019559193
RAB8B	1.64732467	0.009639048
MICU2	1.647283422	0.009039471
ACTR6	1.645770963	0.017601226
DCUN1D4	1.644432166	9.34107E-04
PIKFYVE	1.641707001	0.001439253
ST3GAL6	1.640118035	0.002489938
FBXO28	1.639153445	0.033432878
ADAMTS5	1.638922293	5.83059E-04
PHF6	1.637414197	0.013341094
SEPSECS	1.634739429	0.003632657
RNF217	1.634042823	0.016627063
HIPK3	1.632668207	0.014288719
DUSP4	1.629982293	0.009082288
TRAM1	1.629977138	0.019320286
RBM27	1.629433292	0.026106132
DERPC	1.629178237	0.036530056
BCAP29	1.628131448	0.005625896
NHLRC2	1.627225049	0.001243341
LIG4	1.626469897	0.00282273
ATL2	1.618620392	0.002390782
IDI1	1.617023961	0.0025394
MDM2	1.609655635	0.003868238
DCP2	1.608707426	0.033262511
OSBPL8	1.607394102	0.001974048
ZRANB2	1.605661722	0.009321021
TMEM47	1.604136025	0.024325799
LUC7L2	1.603435737	0.006963304
ATL3	1.603372388	2.40E-05
PURB	1.598197465	0.014288719
TMBIM4	1.598049026	0.013493117
CLIC4	1.597395452	0.001057016
GTF2A1	1.595662795	0.042484503

CKAP4	1.288487979	0.009683072
KREMEN1	1.286156278	0.028013363
EMILIN2	1.282622739	0.045894128
SLC39A7	1.282416066	0.011757098
RPL26	1.280325105	0.014238809
TMEM214	1.280217608	0.018427386
MED22	1.27910003	0.026106132
RPL35A	1.275579681	0.021332314
RPS27	1.274359547	0.015894141
EEF1B2	1.272331772	0.016942113
LSM10	1.271431429	0.040760567
MYL6	1.269838246	0.036724698
PRDX5	1.269463774	0.044944421
RPS17	1.26928268	0.009347295
VAT1	1.26648043	0.005206814
RPL23	1.260933165	0.02116082
RPS3	1.260299066	0.007354994
RPS24	1.260168113	0.032941884
RPL17	1.259266478	0.01092514
RPS15A	1.253976709	0.01912498
RRBP1	1.252634075	0.011601659
MGAT1	1.252485719	0.026617323
TNKS1BP1	1.24851708	0.028712286
RPL27A	1.243141154	0.012249226
RPL41	1.242815945	0.015314576
RPL5	1.241057003	0.016942113
DDOST	1.237748438	0.02570727
FYN	1.236762534	0.049770574
SCPEP1	1.235724713	0.028032884
RPL10	1.235286455	0.028898593
SNHG29	1.233735424	0.029283284
ACTG1	1.231920264	0.002426603
RPL37	1.229314277	0.026055325
EPRS1	1.228872127	0.013722883
CLUH	1.22745724	0.040346461
RPL21P16	1.226798889	0.047024865

GULP1	1.595605018	0.031928688
UBA6	1.593021331	0.001539027
HOOK3	1.590719698	0.00553322
CPEB4	1.590462157	0.008808058
PKD1L2	1.590099549	8.17322E-04
ELMOD2	1.587513998	0.006296086
RAP2C	1.586577114	0.011413955
TMED5	1.584850972	0.006192901
ABCA1	1.584750026	7.53490E-04
EEA1	1.583439055	0.003122399
TRIQK	1.583105171	0.043133858
SC5D	1.582400741	0.001556505
MTMR6	1.581999442	0.016942113
TM9SF3	1.581990015	0.009639048
FKBP5	1.580102928	0.035395303
SLC5A3	1.579918624	0.006963304
MTX3	1.579765755	0.004115189
PPP1CB	1.577991235	0.005059386
UBN2	1.577001512	0.010522132
ZMPSTE24	1.573475471	2.09188E-04
FAM122B	1.573017005	0.016942113
TRHDE	1.568954466	0.004601794
MARCHF7	1.568475017	0.003644521
RUFY2	1.567265966	0.025405348
PLIN2	1.567227007	0.011002491
OTUD1	1.566280804	0.040913186
BROX	1.565459228	0.011002491
METTL7A	1.562509679	7.56036E-04
TIA1	1.557858222	0.004368706
SERP1	1.557155815	0.012249226
COX11	1.553880407	0.013585604
DPY19L1	1.552951305	0.012439817
STK17A	1.547829056	0.044944421
FOPNL	1.54582848	0.023539111
SMNDC1	1.545793434	0.025522559
ABCC2	1.545553196	0.041775496

RPL4	1.225746363	0.007903455
TCTA	1.2225483	0.049770574
RPL23A	1.222208532	0.015370522
PLOD1	1.221005637	0.049770574
RPL24	1.218257091	0.031619639
RPL30	1.217773627	0.034274447
EIF2S2	1.215545229	0.03688443
RPS27A	1.213740363	0.021079473
RPS6	1.203805812	0.021818012
BRD2	1.201551279	0.04113973
RPLP0	1.196485949	0.03360203
RACK1	1.187865836	0.022816791
RPL19	1.178598007	0.038409462
EIF1	1.176885357	0.036000348

TRIM2	1.544446227	0.014513203
FPGT	1.544282701	0.026238504
ARPP19	1.54286851	0.001097841
QSER1	1.541838239	0.033001685
GOLGA8O	1.540004288	0.018338883
OLMALINC	1.539679306	0.024250154
MBNL1	1.539664881	6.66840E-04
ADH1B	1.539492224	8.97402E-04
KIAA0408	1.539438064	0.005540726
LDLR	1.538336557	0.001171324
HS2ST1	1.536064698	0.024742777
SLC46A3	1.535694066	0.01912498
XPO1	1.535237374	0.006192901
ARL8B	1.534776645	0.015426711
EPM2AIP1	1.534304591	0.018338883
TGFB2	1.533522335	0.031458936
LBR	1.531731124	4.09504E-04
ZDHHC17	1.530739172	0.008070796
TMTC3	1.529597025	0.049770574
BTG1	1.528144407	2.44E-05
ELK4	1.528094519	0.007279923
ERI2	1.526963521	0.01537768
TFAM	1.524059226	0.024250154
CCNG1	1.522242215	0.024836407
MIGA1	1.52173338	0.03576755
TXNDC16	1.520833847	0.021612084
PHLDB2	1.519916086	8.43E-06
TAF13	1.519276315	0.01109546
XPO4	1.519250823	0.033432878
UBR3	1.519206277	1.65206E-04
UBE2G1	1.518618599	0.00312802
FAR1	1.517945355	0.001556505
RGPD8	1.517202819	0.012559806
PNPLA7	1.515350056	0.004201784
PPP3CA	1.51454799	0.003644521
ZDHHC20	1.514522854	0.04683534

RAB18	1.514405317	0.015055572
REEP3	1.511186299	0.005568504
PKN2	1.509804565	0.004201784
TP53INP1	1.508282629	0.029636358
RBM26	1.508000473	0.005206814
ARRDC3	1.507441663	0.04798007
RGMB	1.506658251	0.016334304
CERT1	1.505988976	0.005806334
FAM172A	1.505329063	0.006070688
KRR1	1.50528136	0.011874285
SPTY2D1	1.504612481	0.040346461
SMC5	1.503873568	0.026466925
PCMTD2	1.503785249	7.53490E-04
LRRC8C	1.503263053	0.00826203
SLC2A4	1.502229188	0.032587494
CITED2	1.499093967	0.011119651
EXOC5	1.499047552	0.002220415
TFPI	1.49748371	0.047155657
ARMC1	1.496985856	0.040527254
TTC14	1.496242495	0.008432148
PLSCR4	1.49597739	0.002220415
ORC4	1.48915502	0.039271432
FAM49A	1.489124921	0.020997421
MAN1A1	1.487024377	1.84674E-04
BRI3BP	1.486664408	0.016942113
NEAT1	1.485975593	0.029127847
TMEM64	1.485855354	0.013760104
PIK3CA	1.485781431	0.003348141
HERC4	1.485157429	0.002232955
LYPLA1	1.484577856	0.028560907
CD58	1.484444716	0.049637267
PLEKHG6	1.484432909	0.001031618
TMEM168	1.483044595	0.00302837
USP33	1.482493109	5.72864E-04
C2CD5	1.482278008	0.043731112
CGGBP1	1.481901851	0.016833348

LARP4	1.48185135	0.009399688
QKI	1.481065215	0.003450954
TMEM30A	1.480576667	0.013155844
SLC35F5	1.480256747	0.011854469
ATP11C	1.476777453	0.038409462
DNM3OS	1.47651195	0.047029983
SNTB2	1.475918781	0.00511956
RRM2B	1.475796988	0.001057016
VAMP7	1.47293005	0.026238504
BNIP3L	1.471329198	0.010760128
GSDMB	1.46943827	0.020201792
TWF1	1.466759303	0.023010302
LYRM7	1.466149751	0.04543617
COMMD10	1.465963616	0.039825465
PHC3	1.465142593	0.023738859
SLC35A5	1.463162167	0.033132104
MDGA1	1.463118873	0.030894038
UGCG	1.460496889	0.049760059
ZFYVE16	1.459053295	0.023861172
STRN	1.457948588	0.007360533
SRSF11	1.457848262	0.007536663
GET1	1.457637291	0.036000348
ACAP2	1.4573837	0.013101873
XIAP	1.456243301	0.041963184
COX20	1.455879749	0.024831194
PPM1L	1.454966695	0.006558859
KCTD12	1.454772881	0.034954065
DESI2	1.454008556	0.012807519
SMIM14	1.453864267	0.014297669
RB1	1.45324666	0.007359602
SPPL2A	1.451715719	0.025853687
SMAD5	1.451661896	0.020201792
MCFD2	1.44675209	0.010252936
KLHL31	1.446031648	0.016047417
TEAD1	1.44598731	0.004799367

OTUD4	1.443719233	0.007294152
YIPF4	1.442924895	0.021560563
ZNF518A	1.441139288	0.021338695
BRWD1	1.440362122	0.010456752
LNPK	1.44006462	0.048131785
GPAM	1.439732014	0.006535645
MTPN	1.438369157	0.016050364
RWDD4	1.438341258	0.027327849
GLS	1.437953392	0.032054274
SHROOM1	1.437153911	0.045424632
CPM	1.436370245	0.005855202
YPEL5	1.43569492	0.003208808
BHLHE41	1.435601735	1.18625E-04
PTEN	1.434578242	0.03412765
CLIP4	1.434359156	0.001242964
MAGT1	1.434127531	0.008808058
LNPEP	1.434003635	0.01742178
PERP	1.433466015	0.040351813
LGR4	1.429156759	0.018788117
TASOR	1.42890232	0.018788117
RB1CC1	1.426737845	0.008808058
LMAN1	1.421220395	0.043664144
TVP23B	1.420974126	0.024831194
BMP2K	1.420607473	0.04798007
ARMT1	1.420523986	0.032457963
FNBP1L	1.419951075	0.001203766
SLC30A9	1.417978135	0.043124855
LMBRD1	1.417907506	0.013778511
TMEM181	1.415861789	0.00360121
S100A4	1.41573392	0.009757157
FGD5-AS1	1.414894387	0.024250154
NFAT5	1.414448867	0.042129103
BZW1	1.413919465	0.011002491
SERINC1	1.413487391	0.003644521
DMXL2	1.413460352	0.038273638
NEK7	1.413425743	0.010281112

RPS6KA3	1.411968453	0.033903029
FBXL17	1.406964565	0.02384103
C5orf51	1.406870964	0.041008453
GCLM	1.404297521	0.008808058
UBE2E1	1.404007633	0.023701721
KIF21A	1.401322682	0.025107069
POLI	1.400855895	0.013101873
CYCS	1.399567042	0.033432878
RAB21	1.398422583	0.043664144
SCYL2	1.396753573	0.044558703
PPIP5K2	1.396294958	0.037909547
ANKRD46	1.396163385	0.03433825
TMEM123	1.39491985	0.024229262
ACHE	1.394785596	0.013722883
ITGAV	1.394016113	0.033412431
PTGES3	1.393033103	0.034110735
FNIP2	1.393012648	0.01188597
MAP3K2	1.392526033	0.039825465
VPS13A	1.39195845	0.028552743
STAG2	1.391665364	0.021332314
ATRX	1.39151582	0.026636883
BTF3L4	1.391407545	0.021356805
TMEM33	1.390080909	0.024797168
SMAD4	1.389617785	0.009908641
DUSP6	1.38898634	0.045146157
EGLN1	1.388544581	0.033432878
KLB	1.38640613	0.00371082
SEPTIN10	1.3859445	0.045739886
HERC2P9	1.383602031	0.044558703
TBC1D4	1.383380333	0.018427386
RAP2A	1.38314549	0.046308452
MON2	1.381798094	0.046729932
ITPR2	1.3791487	0.009639048
CAB39	1.379079098	0.035854731
PPP3R1	1.377330935	0.041135758
VAMP3	1.377038687	3.63949E-04

SNX13	1.376489443	0.043261735
CFL2	1.376436668	0.03688443
ORMDL1	1.3758604	0.009308089
SQLE	1.374487361	0.038900789
CCNC	1.37420669	0.03412765
JAZF1	1.373992485	0.027815151
MOB1A	1.372522081	0.033593691
DIS3	1.371261388	0.016390349
APOE	1.371074617	0.047028076
VPS26A	1.370618323	0.005245906
RNF13	1.370347791	0.004799367
GOLGA8A	1.370186257	0.027300736
TRPM7	1.368444118	0.03576755
DBP	1.368324916	0.009399688
INSIG1	1.366786911	0.003053242
XIST	1.366488146	0.012439817
DSE	1.365433434	0.028898593
ATE1	1.363872876	0.028560907
ATP6AP2	1.36117733	0.018338883
SREK1	1.360449313	0.012789923
RHOQ	1.360229899	0.006070688
PPM1A	1.359654779	0.004071957
RSRP1	1.359346649	0.007360533
RPE	1.359176304	0.011753657
MYO6	1.358542346	0.035628462
UBE2D3	1.358209493	0.028560907
AGL	1.357780417	0.046009714
CEP350	1.357217347	0.032669855
YTHDF3	1.357152313	0.040527254
RPS6KB1	1.355066512	0.045672991
ATP6V1A	1.353502067	0.009823624
NCKAP1	1.353501706	0.035854731
TM9SF2	1.352217952	0.015426711
ZBTB44	1.351739076	0.020997421
PPP1R12A	1.350200489	0.038686211
TBC1D23	1.349813537	0.034906527

STX7	1.349658404	0.004769713
SDHD	1.348924587	0.016942113
PCYOX1	1.348016765	0.011030916
MINDY3	1.347670133	0.034718462
DYNC2H1	1.344310118	0.033628114
CMPK1	1.343083148	0.047157029
FEZ2	1.342512717	0.042320898
HBP1	1.342398989	0.011326857
CXXC5	1.334992937	0.013850331
BCL2	1.334480628	0.013155844
RHOBTB3	1.334317641	0.028560907
CD46	1.334160193	0.003302134
SPTLC1	1.33388632	0.011792488
CYBRD1	1.332007868	0.038900789
PFN2	1.328560084	0.011995199
CPNE3	1.328128214	0.024007048
SDCBP	1.328050293	0.006850338
PPP2R2A	1.327708383	0.024771952
SLF2	1.327354098	0.044944421
GASK1B	1.327032575	0.024250154
PGRMC2	1.325431339	0.005598489
COG5	1.324559422	0.047431247
PAPOLA	1.324372702	0.040929621
YWHAZ	1.324230154	0.001016624
CPD	1.323737064	0.019291947
VPS36	1.322452717	0.028300232
API5	1.322396543	0.026466925
SNX3	1.322335582	0.022532547
PTPRG	1.321425889	0.030894038
RAB10	1.321229588	0.034069139
RASA1	1.320877965	0.030639646
ATG2B	1.319934754	0.039129216
CYP51A1	1.317979397	0.019322727
CCDC6	1.317971594	0.038158506
HMGCS1	1.31735818	0.046490521
MAOA	1.316252349	0.006192901

ARID5B	1.316234829	0.016134339
PDE3B	1.31553472	0.007228176
CAPZA1	1.312160217	0.023539111
CALD1	1.309794193	0.010252936
PPP3CB	1.309683757	0.034069139
NPTN	1.309626719	0.012906095
EDEM3	1.307672927	0.018267095
UBE2K	1.307256173	0.025987342
PDCD6IP	1.30538612	0.007791431
GHR	1.305151585	0.002706662
KLF8	1.304736741	0.04073497
MATR3	1.303662466	0.027402745
BCLAF1	1.30283702	0.028945193
ZFAND6	1.301887181	0.036000348
SECISBP2L	1.29888784	0.031533858
CSNK1A1	1.296564279	0.020105037
ACTR2	1.295540163	0.011382322
PAFAH1B2	1.29242226	0.027300736
FAM47E-STBD1	1.290510818	0.04073497
SELENOT	1.28938434	0.033412431
HK2	1.286831755	0.001926863
PLOD2	1.285097227	0.03576755
CREBL2	1.280838824	0.046308452
VAPA	1.28045859	0.03738159
RRAGC	1.279814371	0.047612016
CAND1	1.278800798	0.03738159
AK3	1.278057395	0.013493117
STX12	1.276508735	0.047029983
PCDH18	1.276265165	0.001031618
LIMA1	1.275866649	0.038686211
TEF	1.275013884	0.003402445
GALNT1	1.273415974	0.034274447
DENR	1.273268657	0.047029983
STOM	1.270463422	0.031619639
CYLD	1.270308052	0.045894128

NUCKS1	1.268035837	0.044214465
C4orf3	1.267616288	0.027638169
NR3C1	1.264095968	0.04543724
LEPROT	1.262572504	0.025987342
PPP2CA	1.261751273	0.04073497
ACSL4	1.260797494	0.04493747
ASPH	1.259544855	0.045902819
SPG21	1.248301955	0.046308452
PAPSS1	1.247368168	0.046490521
FAM20B	1.246310738	0.024742777
RAB1A	1.245464413	0.043803938
SARAF	1.243789359	0.016942113
B2M	1.243474941	0.024229262
RAD21	1.238615813	0.025853687
GPT2	1.236332093	0.025805872
ZMYND11	1.233429564	0.042222291
TMSB4X	1.232852991	0.03238304
VKORC1L1	1.232724824	0.044944421
PNISR	1.229564793	0.042222291
FMNL2	1.221501302	0.038627334
GLUD1	1.213618942	0.03519073
CCPG1	1.211572037	0.046286624
COQ8A	1.206374061	0.041268881
ZC3H11A	1.19408507	0.04683534
CALM1	1.179350485	0.032054274

TABLE 3. Genes differentially expressed between non-thermogenic and thermogenic adipocytes prior to implantation

Higher in thermogenic adipocytes prior to implantation			Higher in non-thermogenic adipocytes prior to implantation		
Gene	**foldChange**	**log10padj**	**Gene**	**foldChange**	**log10padj**
C2CD4A	155.34	2.57	FABP7	183.54	9.17
LINC00473	109.62	18.19	LTF	122.49	2.85
PTPRN	85.71	35.52	KRT34	70.27	17.88
FGF10	76.55	7.67	KRT19	62.93	31.87
CST2	68.88	5.22	XIRP1	47.05	7.38
AS3MT	63.69	2.33	PKD2L1	45.65	6.69
GPR84	57.23	3.68	TF	43.82	4.40
DLX5	46.37	6.32	ANKRD1	32.84	18.64
FZD10	45.52	2.49	CLEC3B	31.37	17.62
ADCY4	43.43	34.74	PKD1L2	31.28	17.22
PTPN5	39.58	1.68	MYEOV	26.82	6.05
FZD10-AS1	37.75	2.49	KRT33B	26.27	3.83
HPD	37.19	26.51	PSG1	24.87	3.08
FAM71E2	36.56	1.50	AZGP1P1	23.52	4.30
SYT6	35.78	2.57	MYO18B	23.44	3.21
SEMA6B	32.85	5.25	C6	21.98	22.67
VMO1	32.57	25.21	DCSTAMP	21.30	5.03
CLEC2L	32.41	3.28	C8orf34	20.81	19.21
PCSK2	30.73	4.71	TRIML2	19.94	4.32
SERTM1	30.71	4.95	ITIH1	18.99	10.38
ATP2B2	29.77	3.70	SLC14A1	18.79	7.46
SPINK6	29.41	11.76	SERPINB2	18.44	17.93
LGSN	28.64	6.00	LOC286189	18.12	2.10
DLK1	28.63	15.53	NLRP10	18.02	21.72
CD86	28.45	2.53	BIRC3	17.29	28.61
CYSLTR2	27.31	2.17	C1orf95	17.20	29.44
LRP1B	26.82	11.95	HSPA7	16.88	5.14
PCYT1B	25.69	5.49	NMUR1	16.85	21.91
MTUS2	24.87	6.52	KIAA0040	15.98	13.57
DNASE1L3	24.69	12.57	KY	15.89	15.48

VANGL2	24.51	9.64	KRTAP2-3	15.51	19.82
CACNG7	24.49	1.40	NTSR2	15.48	4.12
FNDC1	22.10	48.39	S100B	15.28	7.46
KLRC2	22.03	2.65	RELN	15.06	13.70
CCNJL	22.00	3.32	LOC101929371	14.11	27.35
BAI3	19.88	2.59	ACHE	14.06	61.50
TMEM190	19.72	3.24	FOSB	13.96	6.63
MMP1	19.57	4.94	TM4SF4	13.43	2.45
SNAP25-AS1	17.46	4.93	FCGR3A	12.99	3.53
HUNK	17.38	10.49	LOC100507065	12.72	21.10
TNFSF11	17.06	4.60	APOC1	12.72	15.34
C3AR1	16.56	4.82	HPR	12.49	3.19
ASB4	16.46	1.78	FCRLA	12.37	27.75
MSI1	16.43	3.43	CLCA2	12.21	14.55
OGDHL	15.97	10.45	CD14	11.74	42.93
ASPG	15.45	5.49	MARCO	11.63	4.81
KLRC3	14.78	3.14	PFKFB1	11.60	20.55
DYSF	14.40	15.49	LINC00161	11.49	1.89
BTBD11	14.24	5.09	PRKAG3	10.81	4.07
CCDC177	14.00	3.88	CCR1	10.66	18.24
COL14A1	13.51	25.53	AZGP1	10.62	9.08
FOXF1	13.09	4.03	GRIN2A	10.52	3.96
PF4V1	12.91	4.58	DPF3	10.31	8.36
MATK	12.91	4.12	KRT15	10.26	2.68
VASH2	12.80	6.75	CHRDL1	9.98	14.76
SHH	12.77	1.67	KRTAP1-5	9.90	3.85
TRH	12.38	3.25	ATP1A2	9.89	7.94
SNAP25	12.27	18.40	PHKG1	9.64	84.39
IL18RAP	12.07	5.46	MMP23A	9.61	1.61
PENK	11.94	8.70	FAM19A3	9.22	3.70
LOC101929122	11.75	12.15	ADAMTS8	9.06	5.29
WFDC1	11.65	3.69	MATN2	9.03	15.81
CNTNAP4	11.43	20.72	ITGA8	8.60	17.53
PDE4B	11.34	9.14	ACAN	8.47	2.52

FPR2	11.33	13.77	C14orf180	8.43	3.10
COL10A1	11.27	3.64	LEP	8.33	23.44
NOTUM	11.10	6.31	KRT23	8.27	2.12
CXCL1	10.81	3.88	PTPRR	8.25	6.08
AADAC	10.79	14.99	CHIAP2	8.15	13.61
SPON1	10.71	52.13	GPAM	8.12	25.75
CEND1	10.68	7.92	IL1RL1	8.09	17.09
PID1	10.54	6.28	TRHDE-AS1	8.00	41.59
CRYGN	10.42	6.22	MMP28	7.77	9.71
H2BFM	10.41	2.11	CLDN14	7.76	5.96
HAS1	10.35	5.60	HSPA6	7.73	5.15
FIGNL2	10.33	2.78	NRXN3	7.67	27.15
LRRC15	10.29	15.40	DMBX1	7.65	2.62
TMSB15A	10.20	3.71	KIAA1211L	7.64	2.93
KCNJ6	10.07	3.86	ZG16B	7.58	1.81
HMGN2P46	9.93	1.31	LINC01111	7.53	3.32
SPINK13	9.78	2.10	PPP1R14C	7.46	7.28
CD7	9.77	3.45	AQP7P1	7.45	11.39
TFPI2	9.72	2.84	YBX2	7.39	3.63
MGAT5B	9.72	8.19	ADAMTS16	7.35	12.98
LOC100507195	9.72	2.82	ACVR1C	7.35	11.42
PDK4	9.63	4.89	SLC2A4	7.35	4.87
EFNB3	9.54	12.57	SLC10A6	7.33	1.42
TMEM200C	9.42	3.35	CST6	7.29	2.88
IQCA1	9.28	3.54	ITGB6	7.25	8.70
LSAMP	9.18	17.73	RGS7	7.21	5.26
MEGF10	9.03	2.25	PLCXD3	7.16	11.18
BDKRB2	9.02	5.15	OXTR	7.09	2.99
LOC101927630	9.01	1.42	ADH1B	6.99	9.27
FAM189A1	8.93	3.76	RGS20	6.98	22.16
SEMA6A	8.88	4.66	KCNQ5	6.95	3.04
AQP5	8.81	1.93	SERPINA1	6.89	7.13
KRT81	8.73	2.85	SALRNA2	6.89	7.38
MERTK	8.70	4.40	STRA6	6.86	4.78

SAMD5	8.66	3.56	LHFPL4	6.84	1.69
ENTPD3	8.65	10.15	HHIP	6.81	4.07
NRROS	8.58	5.34	LINC01093	6.78	3.76
TPBGL	8.44	4.91	P2RY12	6.77	2.15
SDC1	8.40	25.19	LINC01119	6.70	38.23
NPTX2	8.35	7.63	GIPC2	6.70	15.39
NDRG4	8.34	6.90	IGSF11	6.67	2.71
FBXO2	8.32	5.42	SCTR	6.66	3.14
PDE3A	8.29	62.72	APOC1P1	6.65	10.13
NPY1R	8.21	4.14	CLDN4	6.63	9.88
ITK	8.17	4.50	CIDEC	6.46	4.42
ST6GALNAC3	7.84	2.96	CA3	6.42	5.35
SLC38A3	7.84	7.12	C7	6.41	9.60
SEMA3F	7.70	9.11	CHI3L2	6.41	3.94
GLI1	7.65	5.66	PRRT4	6.40	11.23
PDE10A	7.62	5.84	CYP1A2	6.37	2.68
OTOF	7.56	10.20	RPSAP52	6.34	26.32
USP43	7.55	2.30	HOPX	6.27	4.09
LINC00622	7.53	5.03	DHRS9	6.25	5.04
FAAHP1	7.51	2.72	ADH1A	6.22	1.64
SPINT1	7.49	2.90	CALB2	6.19	8.45
LIPM	7.47	3.20	RCSD1	6.16	2.95
MGC27382	7.47	1.33	ELOVL6	6.12	26.76
RHPN1	7.45	2.85	USP30-AS1	6.00	1.53
CXCL5	7.45	2.84	LRG1	6.00	5.37
CYP24A1	7.41	1.64	FGD3	5.92	2.19
FAIM3	7.39	2.06	CHST8	5.82	2.62
CXCL6	7.37	3.76	BTLA	5.81	1.59
CXCL3	7.36	2.04	NEK10	5.79	10.07
PRRG3	7.36	2.09	SORBS1	5.75	11.43
CHRDL2	7.36	5.85	SLC7A4	5.71	3.36
B4GALNT4	7.15	11.06	HCAR1	5.67	29.48
TCTEX1D1	7.11	8.55	P2RX1	5.66	1.69
CHGB	7.04	2.45	ACSM5	5.58	13.16
ZFP92	6.99	3.19	LYPD1	5.55	5.27

FAM87A	6.98	6.46	DES	5.53	5.56
PCSK1	6.97	13.94	APOC4-APOC2	5.52	2.38
DAB1	6.89	1.61	RET	5.47	10.46
ENHO	6.88	1.62	MYO7B	5.46	9.32
BZRAP1	6.87	3.26	FMO3	5.44	5.73
GPC3	6.82	62.21	LHCGR	5.44	1.41
TMEM71	6.80	3.36	SERPINA3	5.43	2.21
SLC5A12	6.73	2.48	DIO3	5.41	1.64
LAPTM5	6.72	4.42	MLIP	5.34	1.31
HAPLN4	6.69	5.79	TMEM37	5.33	6.33
KCNH1	6.63	9.68	MTSS1	5.33	15.82
CXCL14	6.61	4.62	ADHFE1	5.30	7.54
PLB1	6.59	4.49	SLCO4C1	5.30	13.90
RUNDC3A	6.59	3.52	CYP1A1	5.28	1.62
FAM43B	6.56	4.19	CASQ2	5.28	4.85
GUCY1A3	6.55	4.79	NPR1	5.24	14.50
TMEM59L	6.55	24.17	C4B	5.23	6.80
TGM2	6.52	15.34	ABCG1	5.22	2.61
TMEM132A	6.43	13.66	PRSS12	5.22	38.78
ENPP6	6.41	1.81	WNT2	5.21	3.14
P4HA3	6.41	23.59	PKP1	5.19	2.52
FMNL1	6.40	20.55	AQP1	5.16	4.21
PDE4D	6.40	11.66	MLXIPL	5.16	6.12
CCL11	6.39	11.65	AGAP11	5.15	18.33
CPT1A	6.35	24.83	PSG5	5.13	2.42
DNER	6.31	2.37	CAMK2B	5.13	4.09
HAP1	6.26	1.53	PLIN1	5.11	8.45
DBNDD1	6.25	4.14	LOC100130476	5.11	3.23
GDF15	6.25	2.25	C8orf46	5.09	3.46
IRF4	6.24	6.61	PPP1R1A	5.07	9.43
EBF4	6.22	4.21	CNTFR-AS1	5.04	2.90
TSPAN11	6.21	5.98	PRSS3	5.01	4.61
SCN4B	6.21	2.19	LRRN3	5.01	14.99
PTHLH	6.20	2.07	ABCD2	5.00	13.86

FOXQ1	6.10	2.65	RGS4	4.97	18.19
NEURL1B	6.08	1.66	CALCRL	4.94	15.96
TM6SF2	6.07	9.19	NEBL	4.93	23.29
SYT3	6.02	2.20	IL7R	4.88	7.56
LCNL1	6.02	4.32	HCP5	4.87	5.57
LOC100506895	5.98	2.01	ABCC12	4.87	2.93
SEZ6L2	5.95	21.02	FMN2	4.82	30.07
CH25H	5.92	6.54	TJP2	4.81	11.23
PRKCZ	5.91	2.20	LPIN1	4.80	31.75
RARRES1	5.89	2.81	AQP7	4.78	9.03
VIPR2	5.88	1.89	TMEM132C	4.78	12.40
PURG	5.87	4.11	KRT18	4.76	1.98
CSGALNACT1	5.84	5.16	IL34	4.76	4.07
SLCO4A1	5.76	1.37	FCN2	4.69	2.34
PCDHA12	5.73	2.44	ORM1	4.69	1.72
NUDT10	5.70	3.42	SCD	4.67	5.74
LOC102723927	5.68	2.28	GPR39	4.65	15.39
EMID1	5.68	1.78	SCEL	4.64	2.36
CRISPLD1	5.67	4.40	GRIA1	4.63	3.47
INSRR	5.62	2.04	LOC100126784	4.61	9.38
SFRP4	5.62	6.12	THRSP	4.61	1.69
NR1D1	5.61	40.04	SEMA3G	4.59	7.40
LPAR4	5.60	2.03	SLC2A5	4.59	2.49
RIPK3	5.58	12.46	DTX4	4.58	14.54
SLC27A2	5.57	2.04	NKD2	4.55	5.23
PF4	5.56	3.37	LOC101929524	4.55	2.18
NTNG2	5.56	25.76	ABCA4	4.54	2.92
CYFIP2	5.56	4.44	TPRG1-AS1	4.52	5.03
PON3	5.55	5.03	GPRIN3	4.51	3.67
ATP2A3	5.48	6.84	LOC100507477	4.51	2.06
ASTN1	5.46	1.81	ADIRF	4.48	5.40
UCP1	5.44	1.53	FRMPD3	4.48	2.64

KIF5A	5.43	1.73	FCRLB	4.47	5.63
OBSCN	5.36	4.21	KCNB1	4.43	8.29
PDE7B	5.36	40.92	PTPRQ	4.43	13.96
CRISPLD2	5.35	6.53	NFATC2	4.40	10.54
PCDH19	5.35	2.47	MICALCL	4.39	2.73
MYO1F	5.34	3.54	ADRBK2	4.39	16.29
SFRP2	5.33	49.31	CRACR2B	4.37	7.13
GPRC5C	5.32	27.14	LINC00341	4.35	12.09
MDFI	5.31	2.78	DKK1	4.34	17.26
PTGES	5.31	6.21	LOC101928882	4.33	2.61
CORO1A	5.29	3.84	IL32	4.31	9.54
CYTL1	5.28	7.81	DSP	4.30	7.35
TENM2	5.25	1.56	FAM47E-STBD1	4.30	4.75
TRPV4	5.22	16.43	RNF128	4.30	4.62
SALL2	5.21	14.61	LOC286297	4.29	7.96
GAS2	5.20	2.59	GFRA1	4.29	2.14
TMEM25	5.19	18.10	SPATA9	4.28	14.21
TNFAIP6	5.16	2.30	AOC3	4.28	9.79
BCAM	5.16	43.57	DAW1	4.25	5.63
ITGAX	5.15	1.53	CSPG4	4.23	10.89
MDK	5.15	26.97	DGAT2	4.22	5.87
IGFBP4	5.11	79.61	ARC	4.21	9.60
MYO3B	5.11	4.75	TRHDE	4.20	31.23
SULF2	5.10	12.85	SYNE3	4.18	16.28
PSD	5.09	12.06	ITIH5	4.17	2.35
AQP9	5.09	5.31	C19orf80	4.17	2.12
SIGLEC9	5.07	2.26	SIGLEC15	4.16	2.73
F7	5.05	2.01	AVPR1A	4.14	9.58
AARD	5.04	2.26	ADRA1A	4.13	4.89
PDPN	5.04	61.86	PTPRB	4.13	3.54
SLC26A10	5.01	4.13	LRFN5	4.12	10.53
EPSTI1	5.00	23.71	PLIN5	4.12	4.90
PRSS35	4.99	7.99	MYZAP	4.08	13.38
RAMP1	4.96	4.89	LOC10050	4.07	4.87

			5635		
PDK3	4.95	32.01	LOC102724550	4.07	3.33
TMEM158	4.93	1.84	GDF6	4.07	6.65
CLVS2	4.90	2.17	HLA-F	4.05	3.88
FAM24B-CUZD1	4.90	1.98	HPGD	4.04	1.31
RYR1	4.90	1.69	AQP3	4.04	4.60
GNAZ	4.89	2.13	AQP7P3	4.03	3.33
PAPPA-AS1	4.89	5.91	MYOZ2	4.02	8.84
BRINP1	4.87	22.75	TEK	4.00	5.31
LTK	4.87	1.39	GPR112	4.00	1.44
LOC653602	4.84	1.90	GOLGA7B	3.99	3.58
TLE6	4.84	6.70	AQPEP	3.99	5.64
BPIFB4	4.83	1.88	NPAS1	3.98	4.20
BEX1	4.83	2.08	CRHBP	3.97	1.53
CYP19A1	4.80	2.03	ALDH1A1	3.97	4.14
ST3GAL5	4.79	15.74	LIPE-AS1	3.96	6.30
SV2A	4.78	10.13	ANXA3	3.96	4.86
C17orf82	4.77	3.98	LRRC2	3.96	3.92
WDR86	4.77	19.91	LOC101927934	3.95	1.62
JPH2	4.76	2.40	NAV2-AS5	3.93	1.50
TMEM150C	4.76	12.41	NAT8L	3.92	3.16
SHC3	4.75	7.44	GPR116	3.92	1.47
CRLF1	4.73	31.80	RASGEF1B	3.89	5.68
ASB9	4.72	3.40	GHR	3.88	9.39
HSD3BP4	4.69	3.21	TSLP	3.86	12.26
ABCB4	4.68	7.43	GCOM1	3.84	5.10
GCNT3	4.68	3.50	FAM47E	3.83	3.18
KIAA1211	4.65	4.48	FMO1	3.81	2.43
PGF	4.65	2.06	UACA	3.80	16.19
ZC2HC1C	4.63	4.02	CPEB1-AS1	3.80	3.79
PODNL1	4.62	5.33	NR0B1	3.80	6.40
NTRK1	4.62	6.23	DUSP2	3.79	4.30
NRK	4.62	6.80	FMO2	3.78	4.08
SP9	4.61	2.16	CPED1	3.77	18.96

APBA2	4.60	16.78	RGMB-AS1	3.77	8.68
PABPC4L	4.58	1.50	CFD	3.76	5.37
NKAIN1	4.58	5.26	FGF5	3.76	32.78
HHIPL2	4.57	5.83	FGR	3.75	3.71
VTN	4.57	2.76	KCNG1	3.74	2.54
TREM1	4.56	11.08	RASGRP3	3.74	1.88
AMOT	4.54	7.62	CPB1	3.74	2.00
CASC15	4.50	5.67	MAP3K7CL	3.73	22.40
PTGER4P2-CDK2AP2P2	4.46	3.91	NGEF	3.70	3.46
C3orf80	4.45	1.72	LINC00211	3.70	1.61
CPLX1	4.45	1.63	KCNN4	3.69	7.36
TTYH2	4.44	10.96	NAV2	3.68	21.36
GPR161	4.42	12.08	LAMB3	3.68	12.13
RNF144A	4.41	11.21	ITGA3	3.67	17.28
LRRC25	4.41	1.73	SEPP1	3.67	16.81
MMP9	4.40	2.55	MYPN	3.65	3.93
RAB27B	4.40	3.09	APOE	3.65	6.61
C15orf48	4.38	5.91	EPB41L4B	3.65	5.45
ZCCHC18	4.36	9.37	PDLIM3	3.63	3.18
SELL	4.36	1.38	FASN	3.62	61.18
PITPNC1	4.36	7.46	CDC42EP4	3.61	8.59
LDLRAD4	4.36	6.40	PLIN4	3.61	4.11
TMEM255A	4.36	2.74	CEACAM1	3.61	4.35
RCAN1	4.34	18.82	HCAR2	3.60	6.85
DLL1	4.32	4.15	SEMA7A	3.59	9.06
NPTXR	4.31	11.56	CSPG5	3.59	3.38
LOC100507639	4.31	1.50	PRODH	3.58	2.14
SERTAD4	4.30	3.39	TNFSF14	3.58	6.77
CAMK2N2	4.28	2.77	METTL7B	3.57	4.46
PRR19	4.26	2.65	CLDN1	3.57	7.10
JAM2	4.24	7.67	LINC00640	3.56	1.73
			LINC01085	3.56	4.77
MEX3A	4.24	13.04	CNTFR	3.55	9.67
FAM160A1	4.20	2.32	ANGPT2	3.55	3.98
CPT1C	4.20	11.85	GDF5	3.54	10.24

PCDHA7	4.20	10.68	PREX2	3.52	9.99
LTBP1	4.19	7.27	44443.00	3.52	9.16
C1orf168	4.15	2.01	RAB3B	3.51	5.61
ATP1B2	4.15	1.66	CITED1	3.50	3.29
LINC00865	4.14	7.51	RNF125	3.49	6.17
SLC38A4	4.14	7.98	MID1IP1	3.49	32.24
GCH1	4.14	12.24	B3GALT2	3.49	1.49
PLEKHG1	4.14	7.40	SLC19A3	3.48	22.73
ICOSLG	4.11	2.17	PRLR	3.47	1.36
NEFL	4.10	8.56	CPNE7	3.47	16.57
44445.00	4.10	8.69	HRASLS5	3.46	2.89
KIF5C	4.07	2.14	LAMP3	3.46	1.74
HMCN1	4.07	10.93	GLYCTK	3.45	17.58
RASD1	4.05	8.45	PAX5	3.44	1.79
EPHB3	4.05	7.32	THBD	3.44	3.23
ANGPTL4	4.04	10.86	AOC2	3.44	7.01
C1orf145	4.04	1.75	NEDD9	3.43	2.57
RERG	4.04	1.75	DTX1	3.43	23.76
PDGFRL	4.03	6.90	PATL2	3.42	2.07
KSR1	4.02	22.29	EGR1	3.42	4.31
LOC101928100	3.98	2.95	SLC4A7	3.41	43.84
LOC100131289	3.98	1.95	PTGER4	3.39	9.95
NFATC4	3.96	11.18	RDH5	3.37	4.74
KCNJ8	3.96	27.06	CRLF2	3.36	1.59
JAKMIP2	3.95	1.57	TRNP1	3.36	19.26
CYP27C1	3.94	7.71	ACACA	3.36	35.90
CNIH3	3.93	1.69	UCP2	3.34	7.51
LINC00689	3.93	1.34	SRCIN1	3.33	5.56
IL18R1	3.92	7.42	C10orf10	3.33	4.55
SH3RF3-AS1	3.92	5.63	AKR1C8P	3.32	3.57
FAIM2	3.91	4.54	CD9	3.31	10.82
GK	3.88	6.19	CARD10	3.31	2.92
PRR5L	3.87	9.39	LPL	3.31	8.42
FAM46B	3.87	4.85	BMPER	3.31	7.00
NTN1	3.86	2.44	CYB5A	3.30	9.81
FUT8-AS1	3.86	6.73	LINC01060	3.30	3.72

PLN	3.82	3.31	CD274	3.29	1.39
PTN	3.82	2.20	GLUL	3.29	28.20
PCDHA11	3.81	1.67	PPARGC1B	3.28	7.91
CA11	3.80	6.80	CIB4	3.27	1.42
SERINC2	3.80	12.90	TSTD1	3.26	2.37
CCDC184	3.78	2.80	HSD17B8	3.26	6.35
RTN4RL2	3.78	9.69	ADAMTS18	3.25	3.29
PNCK	3.78	2.40	SLC7A10	3.24	14.41
COLEC12	3.76	8.01	LINC00704	3.24	2.08
BDKRB1	3.74	4.52	SCUBE3	3.23	3.21
GBGT1	3.74	5.23	ADAMTS9-AS1	3.22	4.54
FLJ46906	3.74	1.76	ERV3-1	3.22	6.33
GJB2	3.74	4.95	GFRA2	3.21	2.80
HHIPL1	3.72	29.11	ATP8B1	3.21	18.12
GDNF	3.71	5.04	CAV1	3.21	38.23
TNC	2.27	3.87	MAPT	3.21	14.09
RNF175	3.70	2.09	SREBF1	3.19	10.40
CLGN	3.69	10.82	C3	3.18	15.41
H2BFXP	3.69	5.08	LINC01140	3.18	11.73
BRSK2	3.68	2.20	IGFN1	3.17	9.10
MAGEL2	3.68	7.00	A2M	3.16	12.89
ARSE	3.67	7.14	CLMN	3.16	6.24
THSD7A	3.66	3.19	LOC100129940	3.14	6.15
FILIP1	3.65	4.11	LOC101926960	3.14	1.36
MOV10L1	3.65	4.22	COL21A1	3.14	2.87
STMN2	3.64	8.83	PODXL	3.13	2.29
EDNRA	3.64	1.35	MYOM1	3.12	10.06
OXCT2	3.64	3.95	WISP2	3.12	2.90
FAM20A	3.64	11.90	IL17RE	3.12	9.30
NR5A2	3.64	2.06	PKD1L1	3.12	1.81
EGF	3.63	6.09	PPP1R1B	3.12	2.32
HIST2H3D	3.63	2.81	SDPR	3.11	3.98
SLC9A7P1	3.62	2.52	SAMD3	3.11	7.82

SOWAHD	3.61	2.09	HMGA1	3.10	4.97
ARHGEF25	3.60	11.68	FOS	3.10	2.62
EFHC2	3.60	3.49	ADAMTS1	3.10	31.48
DNM1	3.58	5.14	VNN1	3.08	1.91
TRPC3	3.58	1.65	ALPL	3.08	6.96
E2F2	3.58	2.30	ANK3	3.07	2.27
MAP6	3.56	11.91	HTR2B	3.07	2.46
PPAP2A	3.56	7.52	ATP10A	3.04	4.14
DOK6	3.56	10.68	KCNE1	3.04	2.37
SH3PXD2B	3.55	7.51	GRB14	3.04	3.51
GAL	3.54	1.74	MTURN	3.04	13.92
TCF21	3.54	3.17	LIN7A	3.04	5.20
MT1F	3.53	1.82	ZNF117	3.03	8.83
MASP1	3.53	36.64	SHMT1	3.03	3.88
STAB1	3.53	5.44	AP3B2	3.02	4.19
BDNF	3.52	7.17	LINC01204	3.02	5.30
PLD1	3.52	8.71	SERPINB7	3.01	11.98
SHC2	3.51	3.60	CLSTN2	3.01	5.34
TCF24	3.51	1.39	FOXL1	2.99	12.41
SMOC1	3.51	1.33	GPD1	2.98	1.79
RIMKLA	3.50	2.91	PNPLA3	2.98	7.93
HYAL1	3.49	4.76	VWF	2.97	4.57
RASSF5	3.48	10.57	KCNS2	2.97	7.29
SALL4	3.48	2.81	CTB-113P19.1	2.96	3.31
SYT11	3.48	21.61	SLC25A18	2.95	4.65
CLIC6	3.47	2.86	DNAH5	2.95	5.35
HAS3	3.47	4.96	LOC100132215	2.95	6.20
COL8A2	3.47	6.70	TYRO3	2.95	21.87
LCP1	3.47	2.29	SYN2	2.94	7.55
TSPY26P	3.46	4.85	TIMP3	2.94	3.28
LOC375196	3.45	1.37	CBR3	2.93	30.45
PLXDC2	3.45	6.59	LGALS12	2.93	2.81
COL24A1	3.45	15.36	CYP4F12	2.92	4.43
SHF	3.43	5.12	PPP2R5A	2.92	12.11

WNT5A	3.43	4.31	FAM186A	2.91	2.39
GUCY1B3	3.43	18.19	HK2	2.91	14.26
E2F8	3.42	2.52	MGLL	2.91	10.11
BMP6	3.40	3.47	FOXP4-AS1	2.90	1.40
HR	3.40	4.23	PLEKHA7	2.90	8.04
SLC16A4	3.39	11.08	AOC4P	2.90	1.89
PXDNL	3.38	1.48	SNORA6	2.89	1.94
CASC10	3.38	7.01	NHSL2	2.86	4.59
CA9	3.36	2.23	MAP2	2.86	14.49
MAP3K9	3.36	2.70	AIM1	2.85	4.00
DOCK4	3.36	3.64	RGMB	2.85	9.07
EDIL3	3.35	5.77	ALS2CL	2.85	2.56
KCNE4	3.35	18.79	ACSL1	2.85	6.17
GRASP	3.33	13.11	LINC00944	2.84	1.46
SHANK1	3.33	4.46	FAM213A	2.83	14.34
IMPA2	3.31	14.08	TPRG1	2.83	22.25
IGFBP2	3.31	4.32	WNK4	2.82	4.44
BAI1	3.31	1.56	CARD16	2.82	4.97
CHI3L1	3.31	1.50	G0S2	2.81	7.65
TMEM121	3.30	3.77	KLHL4	2.80	2.08
GPR183	3.30	2.15	AGPAT2	2.80	7.39
FAXC	3.30	2.04	NNAT	2.80	4.63
PACERR	3.29	1.55	ARHGAP29	2.80	7.81
CCL26	3.29	3.69	LRRN4CL	2.80	5.19
WNT3	3.29	10.37	SH2D3C	2.78	2.01
ZDHHC19	3.29	1.42	LOC100128317	2.78	2.06
MAP7D2	3.29	3.23	ZNF608	2.75	32.84
GNA14	3.28	5.58	FOXC2	2.75	6.85
PAPPA	3.28	15.14	LOC102723701	2.75	2.36
BRSK1	3.27	9.77	ABI3BP	2.75	2.57
LOC100506674	3.27	3.33	ABCB5	2.74	2.17
DCAF12L2	3.26	1.44	NRG1	2.73	5.11
RFX8	3.25	3.74	DNAJB4	2.73	11.87

SMOX	3.24	5.85	LAMC2	2.73	8.21
ITGA10	3.24	3.23	HP	2.72	4.11
APLP1	3.23	18.16	KCNA1	2.71	1.31
ZDHHC14	3.23	5.13	APCDD1L-AS1	2.71	3.93
SCD5	3.22	9.72	EFCAB3	2.71	3.08
LINC00887	3.21	3.63	ARNT2	2.70	26.15
SLC39A8	3.20	6.56	LINC00260	2.70	4.32
NYAP1	3.19	2.71	LAIR1	2.70	2.46
PTGFRN	3.19	15.12	PRKAR2B	2.70	3.96
GRAMD1B	3.18	2.36	SYN1	2.69	4.51
VCAN	3.18	10.56	ARHGEF16	2.69	2.15
CMPK2	3.17	2.31	RPS6KA6	2.69	19.14
HVCN1	3.17	5.26	ITGA7	2.69	4.12
GJA1	3.17	47.16	ADIPOQ-AS1	2.69	1.88
KRT80	3.16	3.06	STK32A	2.67	8.47
SLC43A3	3.15	9.57	HPN	2.67	1.54
GALNT12	3.14	7.46	HLF	2.66	1.82
GPR3	3.14	3.17	ZNF560	2.66	1.91
LCTL	3.14	1.53	C10orf105	2.66	1.69
MEX3B	3.14	5.61	HLA-B	2.66	2.56
ZBED6CL	3.14	4.66	PLA2G16	2.66	5.29
RELL2	3.13	6.17	FXYD1	2.65	2.45
FAM87B	3.13	3.16	ZNF571-AS1	2.65	4.59
HTRA3	3.13	7.10	PLEK2	2.65	1.92
GALNT15	3.13	11.49	PRUNE2	2.65	4.10
FAM124A	3.12	7.00	FMN1	2.65	5.58
ACSL4	3.12	3.71	CCL20	2.64	2.44
MAP2K6	3.11	2.49	PLA2G6	2.64	7.15
DIO2	3.10	4.92	ME3	2.64	2.90
PANX2	3.08	6.46	KLF15	2.63	5.11
OLFML3	3.08	17.62	C9orf43	2.62	1.97
TLL1	3.08	1.93	EGLN3	2.62	2.81
DMBT1	3.08	1.52	SLC1A7	2.60	3.33
GIPC3	3.07	2.20	C12orf56	2.60	2.07

HTR7	3.07	1.94	PTGER3	2.60	9.26
TMEM255B	3.06	2.35	ADIPOQ	2.59	2.18
TLE2	3.06	13.81	ABCC2	2.58	1.79
HIF1A-AS2	3.06	4.40	NRCAM	2.58	7.68
FER1L5	3.06	1.61	SPDL1	2.57	26.92
LRP4	3.06	3.82	TMEM170B	2.57	3.36
HECW1	3.06	5.31	loc920	2.56	6.47
TCEAL7	3.05	10.20	STX11	2.56	3.52
PCDHB8	3.05	9.47	ACKR1	2.56	5.60
ABTB2	3.05	14.69	PCK1	2.56	2.47
PAFAH1B3	3.05	14.60	BLOC1S1-RDH5	2.55	2.00
KCNE1L	3.05	2.05	MBL1P	2.55	2.33
ZNF853	3.02	5.75	DOCK10	2.55	13.33
HIF1A-AS1	3.02	7.01	APOD	2.55	19.48
PRTFDC1	3.01	4.16	PTX3	2.54	3.31
C14orf37	3.01	17.72	HMGA2	2.54	6.09
FGF11	3.01	2.18	SNORA52	2.54	1.54
HSD11B1	3.01	1.56	S100A3	2.53	5.61
TUBB2B	3.00	2.09	PTPRF	2.53	4.92
P2RY6	3.00	2.01	P3H2	2.53	7.38
PTPRN2	3.00	1.81	MESP1	2.53	2.43
NXN	2.99	14.16	LRRC8C	2.53	15.01
NEGR1	2.99	15.84	PLXNA2	2.53	6.02
JAKMIP3	2.98	3.64	INHBB	2.53	8.75
OPRL1	2.98	4.68	TM7SF2	2.53	7.14
PTP4A3	2.98	6.63	LOC100507002	2.52	1.62
PBK	2.97	4.17	ADCY5	2.52	2.75
GPR162	2.97	8.62	TCF7	2.51	3.39
RSAD2	2.97	1.58	STAT5A	2.51	14.36
PPARGC1A	2.97	13.51	SORT1	2.51	9.34
PLCB1	2.97	4.18	CDH23	2.51	3.76
LOC100129973	2.96	2.02	FERMT1	2.51	4.90
AFP	2.96	2.57	EHD1	2.51	25.65
RARB	2.96	1.59	KIAA0408	2.51	3.88

ROR2	2.96	53.70	ALDH1A3	2.51	18.98
FLJ22447	2.95	4.32	PLCE1	2.50	3.25
PTGDR	2.95	2.06	DBNDD2	2.50	10.01
LPAR1	2.94	13.05	PCOLCE2	2.50	4.40
FBXO41	2.94	7.26	MAOA	2.50	13.88
KYNU	2.94	1.97	KLB	2.49	2.82
TROAP	2.94	4.05	SLITRK2	2.49	3.15
PCDHA4	2.94	3.99	LINC00673	2.49	1.81
MEGF6	2.93	5.22	PARP12	2.49	12.27
IFI30	2.93	17.33	LINC00693	2.49	1.33
SMO	2.93	40.37	GPR126	2.48	1.73
GPR85	2.92	13.01	FAM180A	2.48	6.51
MFSD2A	2.92	10.10	ZNF300P1	2.48	9.43
MYO15B	2.92	2.95	ANKRD33B	2.47	3.06
ARAP3	2.92	11.06	AGMO	2.47	2.51
NIM1K	2.91	6.70	GYG2	2.47	7.10
PLP1	2.91	3.07	IGFBP3	2.46	4.09
CHST6	2.90	8.63	RCAN2	2.46	4.99
EDNRB-AS1	2.90	2.06	OR7E12P	2.46	5.09
DLG3	2.89	9.07	IZUMO4	2.46	3.13
PCDHA13	2.89	1.62	STON1	2.46	9.44
TBX2-AS1	2.88	3.79	CP	2.46	1.82
TRIM46	2.88	8.77	KIF21A	2.45	14.84
CDH24	2.87	8.70	ZNF474	2.45	1.59
UBE2QL1	2.87	1.93	FST	2.45	5.76
CYP26B1	2.86	1.65	C11orf91	2.43	2.36
MARCKSL1	2.86	10.84	ERRFI1	2.43	5.87
IGDCC4	2.86	4.46	DCBLD2	2.43	26.40
CD1D	2.86	4.23	THSD4	2.43	5.31
HIC1	2.85	4.93	SBF2-AS1	2.43	5.67
DACT3	2.85	7.99	DBI	2.43	11.28
GAL3ST4	2.85	11.08	C10orf128	2.43	1.51
FAM66B	2.85	1.55	PRPS1	2.42	6.34
GAS1	2.85	7.84	CKB	2.41	3.02
ANTXR1	2.85	14.50	KRT8	2.41	1.39

FLG-AS1	2.85	4.90	TMEFF2	2.41	1.98
RASSF2	2.85	3.25	FABP5	2.41	6.54
LOC101927188	2.85	2.76	MKRN2OS	2.40	1.64
AXIN2	2.85	13.34	PPP2R1B	2.40	8.33
ETV1	2.84	2.91	PLAT	2.40	21.55
STYK1	2.84	1.64	AATBC	2.39	1.53
ELMO1	2.84	2.64	ITGBL1	2.39	4.20
NR4A3	2.84	5.93	PTGER2	2.39	10.13
MYBL2	2.83	4.37	CCBE1	2.39	5.76
RNF24	2.83	32.51	FRMD5	2.39	3.66
TSPAN18	2.83	1.92	LRRC8B	2.38	22.44
CASZ1	2.83	1.63	MYLIP	2.38	7.03
NUSAP1	2.83	5.07	SLC2A8	2.38	2.86
SLC16A13	2.82	3.66	PIK3C2B	2.38	7.32
TM4SF19	2.82	2.31	C9orf47	2.38	2.43
HHAT	2.81	9.32	SYNGR2	2.38	3.62
KIAA1462	2.81	6.13	MYCBP2	2.38	18.87
FMOD	2.81	5.46	WHAMMP1	2.37	8.70
SLC2A10	2.80	44.43	PNPLA2	2.37	3.56
ASPHD1	2.79	4.62	LPCAT3	2.37	4.93
PELI2	2.79	9.92	CA2	2.36	4.03
IFI6	2.79	4.60	LINC00632	2.36	5.23
MYOZ3	2.79	1.75	FADS1	2.36	14.23
RAB17	2.79	2.76	FRMD3	2.36	4.78
EGFL7	2.79	12.03	RBP4	2.36	2.35
CFAP58	2.78	2.31	ORMDL3	2.35	14.88
MMP11	2.78	3.12	EML6	2.35	4.79
ITPRIP	2.77	3.25	KCNQ3	2.35	2.95
RAG1	2.77	3.29	CAV2	2.35	16.10
FSCN2	2.77	1.71	DNMBP	2.34	22.64
PIP5KL1	2.76	4.06	CCDC80	2.34	2.75
SYNGR1	2.76	5.60	PRSS23	2.34	2.21
TWIST2	2.76	29.15	PIK3R1	2.34	28.43
TC2N	2.76	2.84	CHN2	2.33	2.37
RNF122	2.75	5.51	TSGA10	2.33	6.27

PRKCH	2.75	15.22	ADCY1	2.32	3.65
ELN	3.16	5.31	SBSN	2.32	2.47
NOTCH3	2.75	6.22	WNT5B	2.32	15.75
PLXNC1	2.75	1.89	PODN	2.32	2.27
B3GALNT1	2.75	12.26	LBHD1	2.32	6.93
EPHA2	2.74	3.28	RARRES3	2.32	13.38
CECR6	2.74	2.20	ALDH1L1	2.32	1.79
SH3RF3	2.74	11.55	PLCXD1	2.32	4.32
ANGPTL2	2.74	11.44	LRIG3	2.31	4.26
FLG	2.74	5.39	GPR176	2.31	13.18
ZNF93	2.73	15.84	BOK	2.31	12.33
LINC01050	2.73	1.86	SOS1	2.31	9.58
BZRAP1-AS1	2.73	1.65	LOC79160	2.31	1.68
CFAP69	2.73	14.73	LMO7-AS1	2.31	2.27
TRIM6	2.72	2.28	CDR1	2.30	6.00
SLC4A3	2.72	20.12	CITED2	2.30	8.71
SLC45A3	2.72	3.69	FGF1	2.30	5.40
FAM110B	2.72	4.21	ARNTL	2.30	14.54
KIAA1522	2.71	12.33	MET	2.29	28.00
SFRP1	2.71	14.16	PPARG	2.29	4.42
TOP2A	2.71	6.65	MED12L	2.29	2.35
PIK3CD-AS2	2.71	1.36	VEGFC	2.29	20.70
PIK3R3	2.71	6.93	LINC00264	2.29	1.50
NYNRIN	2.70	18.43	FRMPD4	2.28	1.42
PROB1	2.70	2.05	CD83	2.28	5.24
FER1L6	20.46	3.64	ADAMTSL3	2.27	1.75
EYA1	2.70	2.48	FABP4	2.27	2.06
ENOX1	2.69	7.80	ADRA2C	2.27	1.73
WDR62	2.69	5.58	CEBPA	2.26	3.06
FER1L4	2.68	2.78	PSMB8-AS1	2.26	2.86
SLC7A7	2.68	5.20	FGD4	2.26	2.28
GPC2	2.67	4.64	ITGA6	2.26	1.86
YPEL4	2.67	2.34	SLC36A2	2.25	1.36
C19orf26	2.67	4.73	LOC152225	2.24	1.32

FAM81A	2.67	3.81	FHL1	2.24	13.34
AGRN	2.66	19.86	WFDC21P	2.23	3.41
ADRA2A	2.66	20.47	ACACB	2.23	2.99
COL9A3	2.66	3.00	NMNAT2	2.22	13.50
MMP2	2.65	32.06	ZNF274	2.22	8.82
TRAF5	2.65	7.00	KLF4	2.22	11.51
CADPS	2.65	4.35	LOC101929679	2.22	1.32
TBX2	2.64	3.82	WDR93	2.21	1.36
RRM2	2.64	5.36	HCAR3	2.21	2.97
PRRG2	2.63	1.98	ACSS2	2.21	5.39
PCDHB3	2.62	2.39	TRPC4	2.21	2.06
SLC24A2	2.62	1.57	LINC01279	2.20	2.16
PROCR	2.62	3.00	EMP1	2.20	35.86
SORL1	2.61	1.96	ACER2	2.20	8.29
MIAT	2.61	2.45	METTL7A	2.20	2.81
MRVI1	2.61	5.70	CDKN2C	2.20	3.36
PCDHB10	2.61	10.44	CLDN11	2.19	6.43
PTK7	2.61	4.36	LOC100288798	2.19	3.03
TNFSF10	2.61	2.30	ADCY10	2.19	1.86
CHMP1B	2.61	3.75	ZBTB16	2.19	2.55
LOC100132111	2.61	1.69	SIT1	2.19	1.97
CTSS	2.60	2.05	FRMD4A	2.19	24.44
CLEC11A	2.60	32.23	OLFM2	2.19	5.27
C9orf50	2.60	1.94	SCG5	2.18	5.46
CDK1	2.60	3.47	ASAP2	2.18	23.67
ITM2C	2.60	26.53	CMYA5	2.18	5.61
CACNA1G	4.33	7.21	HAVCR2	2.18	6.60
LPAL2	2.59	5.13	ARRB1	2.17	4.35
HMOX1	2.58	7.53	CD36	2.17	4.80
LEPREL2	2.58	30.08	44258.00	2.17	2.95
HIF1A	2.58	52.71	HEATR4	2.17	1.62
SARM1	2.58	6.34	CSAD	2.17	9.19
FZD2	2.58	11.39	NAV3	2.17	5.86
MLLT11	2.58	33.83	CADM3-AS1	2.16	1.59

MICAL1	2.57	13.58	MICAL2	2.16	3.38
PCDHA6	2.57	2.19	LOC101926940	2.16	1.46
SRGAP3	2.57	6.43	HBEGF	2.16	3.03
LONRF2	2.57	3.96	TNFAIP3	2.16	4.67
SSPO	2.57	2.54	MCAM	2.15	14.48
CIB2	2.57	4.86	LDLRAD2	2.15	3.85
CLIC3	2.57	1.98	ALDH6A1	2.14	9.47
TMSB15B	2.57	2.72	CDC42EP3	2.14	2.53
CIART	2.56	3.89	CASP1	2.14	2.93
DAB2IP	2.56	12.13	MBOAT1	2.14	3.02
IGLON5	2.55	1.37	MMRN2	2.14	1.55
SLC2A9	2.55	4.32	SYNE2	2.14	14.36
ADRA1D	2.55	1.63	IFIT2	2.14	6.53
ETV4	2.55	1.62	SLC29A1	2.14	2.77
AMPH	2.53	8.73	GCHFR	2.13	6.52
RGAG1	2.53	1.76	SMG7-AS1	2.13	1.89
FCER1G	2.53	2.43	ZNF295-AS1	2.13	1.63
KIF26B	2.53	3.91	PCYT2	2.12	53.41
IER5L	2.53	8.98	ARRDC4	2.12	3.30
PCDHAC2	2.52	1.95	DUSP6	2.12	8.22
KIAA1549	2.52	5.80	EEPD1	2.12	5.08
ANKRD65	2.52	2.81	COBLL1	2.12	3.55
NAMPT	2.52	1.40	PC	2.12	6.74
QPCT	2.51	5.27	HILPDA	2.12	3.06
SLC22A17	2.51	14.69	F11R	2.11	2.38
ACTR3C	2.51	1.34	LOC100128398	2.11	6.70
SNX32	2.51	3.07	PEX11A	2.11	6.61
CDKN3	2.51	4.43	AGPAT9	2.11	2.03
GLT8D2	2.51	12.55	CFAP70	2.10	6.89
CIT	2.50	5.50	SVILP1	2.10	2.25
TTYH3	2.50	45.48	SIM1	2.10	4.02
TLL2	2.49	2.02	LOX	2.09	2.93
ADAM23	2.49	2.34	SLCO2A1	2.09	2.68
FHOD3	2.49	20.90	TSPAN2	2.09	2.08

DNAJC12	2.48	15.52	CDO1	2.09	9.13
AUTS2	2.48	6.87	APOL6	2.09	4.02
CSMD2	2.48	9.70	IL6ST	2.08	8.31
PRICKLE1	2.48	13.89	KCNIP2	2.08	1.88
OLFM1	2.48	5.72	ARHGAP22	2.08	11.17
LINC00086	2.48	2.37	TCEA3	2.08	5.80
PLAU	2.47	7.88	OXCT1	2.07	4.93
FAM83D	2.47	3.79	GPATCH11	2.07	13.73
ADORA1	2.47	2.49	OSBPL8	2.07	8.58
PTPRU	2.46	4.28	COL5A3	2.07	7.30
ZNF703	2.46	8.00	HACL1	2.06	15.88
SLC16A14	2.45	1.35	AR	2.06	17.68
LAMA1	2.45	5.61	LRIG1	2.06	6.23
PCDHB16	2.45	6.77	ELOVL5	2.06	9.00
GAP43	2.44	3.51	FADS3	2.06	7.87
APOBEC3B	2.44	2.34	BTG2	2.06	9.88
PCDHB14	2.44	17.93	GREB1L	2.05	2.33
CAMK2A	2.44	5.24	C2CD2	2.05	12.31
KLF9	2.43	6.44	LONRF3	2.05	5.49
CXCL16	2.43	1.73	DMRTA1	2.05	1.93
KCND1	2.43	7.18	ICA1	2.05	1.92
SLC22A18	2.43	11.23	ATP2B4	2.05	4.94
GNG11	2.43	2.76	LYSMD4	2.04	6.79
GALNT5	2.42	19.16	FAM13A-AS1	2.04	3.00
FBXL7	2.42	7.75	F2RL1	2.03	1.90
MX2	2.42	6.16	SMURF2	2.03	14.45
FAM19A2	2.42	1.40	CDHR3	2.03	3.28
MPP2	2.42	2.46	ZFP36	2.03	5.02
RHOB	2.42	3.87	SNN	2.03	6.77
RASIP1	2.42	2.82	SERPINE1	2.03	1.82
TNS4	2.42	2.52	TNFAIP8L3	2.03	2.27
CNTN3	2.41	10.62	CADM3	2.03	3.48
PNMAL2	2.41	5.85	SLC25A21-AS1	2.03	2.45
SRRM3	2.41	4.55	MSR1	2.03	1.33

CTTNBP2	2.40	1.53
AURKB	2.40	3.68
MEIS1	2.40	6.05
OLFML2B	2.40	10.21
SAPCD2	2.39	1.51
RAET1G	2.39	6.15
EPHB4	2.39	28.64
DTX3	2.39	3.86
SEMA3B	2.39	9.01
CKMT1B	2.39	1.82
PARP15	2.38	2.97
FZD1	2.38	7.22
THBS2	2.38	16.72
PHLDA1	2.38	2.71
HLA-DPB1	2.38	4.37
NRP2	2.38	8.11
CACNA2D2	2.37	1.89
ATP8B3	2.37	1.42
NBL1	2.37	4.61
STMN1	2.37	8.15
FAM26F	2.36	1.95
IQGAP3	2.36	5.19
ASPHD2	2.36	3.48
B4GALT1	2.36	40.74
PCAT6	2.36	6.30
KIF14	2.36	4.22
KIF20A	2.36	3.53
ACTG2	2.35	1.72
CTSC	2.35	7.44
HES1	2.35	2.66
RAP1GAP	2.34	1.36
LINC01305	2.34	2.57
CD163	2.34	4.55
RADIL	2.34	1.32
IGSF3	2.34	2.28
KLF8	2.03	3.85
ACER3	2.03	18.41
SLC27A3	2.03	4.66
SYNM	2.02	1.52
CXorf57	2.02	4.64
MALL	2.02	2.74
GLDN	2.02	1.82
KL	2.02	1.73
BST2	2.02	2.37
TUSC5	2.01	1.65
CEBPB-AS1	2.01	1.91
JADE1	2.01	4.50
PRORSD1P	2.01	5.12
ROBO4	2.01	1.45
NETO2	2.01	4.01
ADCY10P1	2.01	4.59
HSPB2	2.00	20.44
SLC7A6	2.00	10.28
TST	2.00	8.33

MRO	2.34	1.96
NBPF25P	2.34	6.39
PCDHB12	2.33	3.10
SLC7A2	2.33	3.14
TMEM217	2.33	4.03
GPLD1	2.33	2.44
GCNT4	2.33	3.61
CLSTN1	2.33	37.64
C1orf233	2.32	2.08
CDS1	2.32	1.99
ELOVL3	2.32	4.40
DISP2	2.31	1.47
OIP5	2.31	2.57
MAGEE1	2.31	6.62
CCNB2	2.31	4.22
ZC3H12A	2.31	3.35
ARSI	2.31	28.65
RNF39	2.31	2.02
LINC01011	2.31	3.53
MAP3K12	2.30	11.93
EXPH5	2.30	1.53
RAB3A	2.30	3.26
SLC17A7	2.30	1.41
CES4A	2.30	7.18
PCDHB18	2.29	1.30
ECM1	2.28	9.29
PCDHB2	2.28	16.30
RHOJ	2.28	5.54
CABLES1	2.27	3.57
CCDC136	2.27	21.86
NHLRC4	2.27	2.26
PAPPA2	2.27	9.65
PCDHB11	2.27	1.94
BIRC5	2.26	4.55
PART1	2.26	1.45
CDK17	2.26	2.60

LIMS3L	2.26	1.83
SLC37A1	2.26	4.81
ZFYVE28	2.25	10.64
AKR1B1	2.25	4.44
SLC6A10P	2.25	1.89
LOC440895	2.24	1.31
COLEC11	2.24	2.67
SLC44A1	2.24	19.69
DLGAP5	2.23	3.44
HEPH	2.22	6.52
KIF2C	2.22	5.33
CCDC102A	2.22	4.75
C18orf65	2.22	1.81
MRGPRF	2.22	3.96
HIST2H2BA	2.22	1.48
NLGN2	2.22	46.91
TNFRSF10D	2.22	3.04
BICC1	2.22	25.34
WDR86-AS1	2.22	2.27
EPDR1	2.21	9.75
CENPM	2.21	2.71
NCAPH	2.21	3.44
LURAP1	2.21	2.18
FAM171A2	2.21	5.46
NOV	2.21	1.53
RHOD	2.21	5.11
PRL	2.21	1.84
ASIC1	2.20	15.55
FGF7	2.20	72.45
ATP6V1G2-DDX39B	2.20	1.45
DEPDC1	2.20	2.95
FUCA1	2.20	2.48
SRPX2	2.20	38.89
ENO2	2.20	6.70
PLEKHG5	2.66	1.85
LTBP3	2.20	32.15

GSC	2.20	2.50
LPPR4	2.20	1.93
ARHGAP4	2.19	2.01
RPS6KA1	2.19	2.90
STAP2	2.19	1.95
LRRC32	2.19	10.54
PCDHGB3	2.19	7.75
SEC14L4	2.18	1.58
MUC1	2.18	1.71
E2F1	2.18	2.51
ATL1	2.18	11.61
NOTCH2	2.18	7.81
OSCAR	2.18	2.75
PKMYT1	2.18	1.77
PTGFR	2.18	2.04
SLC6A9	2.18	2.57
SHOX2	2.18	9.19
ERG	2.17	1.31
RGS14	2.17	5.24
TRIM9	2.17	2.32
MESP2	2.17	1.30
RAB23	2.17	47.39
CDC45	2.17	2.14
FOXM1	2.17	6.02
PSRC1	2.17	2.86
LOC100506188	2.16	3.59
CBX2	2.16	1.85
LIPG	2.15	1.63
NOL4L	2.15	6.16
EPOR	2.15	4.42
FAP	2.15	35.43
MRAP2	2.15	1.35
ANKRD6	2.15	8.26
FZD3	2.15	9.61
TGFBR3	2.15	5.61
ARHGAP5-AS1	2.14	2.28

DPYSL3	2.14	8.39
RAB43	2.13	5.02
RBM47	2.13	11.86
GREB1	2.13	2.39
PDGFRA	2.13	18.88
GDNF-AS1	2.12	1.37
GTSE1	2.12	3.32
FOXRED2	2.12	12.89
SNED1	2.12	1.75
SPTBN2	2.12	1.96
CTNNB1	2.12	8.19
CENPF	2.12	3.92
NACAD	2.12	1.57
S1PR1	2.12	5.19
AGPAT4	2.11	3.42
SUSD5	2.11	3.79
TEC	2.11	1.76
ZNF439	2.11	3.72
CCDC88B	2.11	1.53
PCGF2	2.11	5.82
WIPI1	2.11	11.25
FAM64A	2.11	1.90
BACH2	2.11	3.98
PRRX1	2.11	12.51
LOC101927780	2.11	5.13
GLB1L2	2.10	2.70
MAPK8IP1	2.10	12.00
BOC	2.10	14.91
UBE2C	2.10	3.50
PCDHB9	2.10	5.63
PCDHB6	2.10	2.90
LIMS3-LOC440895	2.10	2.44
LRCH2	2.10	3.98
ADAM33	2.10	2.26

SLC6A6	2.09	2.70
STOX2	2.09	1.82
IFITM1	2.09	5.91
GPSM2	2.09	14.42
IL4R	2.09	3.66
LINC00888	2.09	3.02
COL11A1	2.09	1.81
TGFBR1	2.09	8.26
OASL	2.08	2.97
SETBP1	2.08	5.11
TBL1X	2.08	6.66
KRT7	2.08	1.77
TBX5	2.08	2.23
ESCO2	2.08	1.32
ADAM28	2.08	1.77
ANKRD29	2.08	2.55
EXO1	2.07	2.21
RAD54L	2.07	2.24
PROCA1	2.07	1.56
ZNF462	2.07	11.55
ADAMTS14	2.07	3.26
TMEM35	2.07	4.54
PDE1A	2.07	5.18
SHROOM4	2.07	1.88
CD55	2.07	11.66
GAREML	2.07	5.41
KIF4A	2.06	2.79
MAGIX	2.06	2.18
HFM1	2.06	1.72
PDIA4	2.06	14.99
CLSPN	2.06	2.14
FRAT2	2.06	4.38
FIBIN	2.06	1.56
TSHZ2	2.05	8.76
LUM	2.05	17.04
KIFC1	2.05	3.66

ANGPT1	2.05	11.37
PCDHB4	2.05	4.80
LINC00965	2.05	2.87
KIAA0101	2.05	3.59
IL15	2.05	2.36
CD101	2.04	1.36
CCNE1	2.04	3.96
WIPF1	2.04	6.90
COL18A1	2.04	3.61
AZIN2	2.04	6.93
MAB21L1	2.04	2.05
C1orf101	2.04	2.95
PCDHB13	2.04	5.28
VGLL4	2.04	8.70
PGM2L1	2.03	3.59
RCOR2	2.03	2.50
SLC6A16	2.03	2.47
CHST14	2.03	26.92
LOC101928796	2.03	2.64
KIF18B	2.03	2.17
DNMT3B	2.02	6.35
PLEKHA5	2.02	3.20
APOBEC3F	2.02	5.63
TRIM62	2.02	10.82
ISYNA1	2.02	2.63
BNC2	2.02	13.26
GLA	2.01	13.42
RAB3IL1	2.01	15.46
GAA	2.01	13.98
STAR	2.01	1.50
CYP2E1	2.01	1.52
CCNA2	2.01	4.65
CEP55	2.01	1.75
PDIA5	2.01	5.38
IFT81	2.01	23.73
ARMC12	2.00	1.31

PARD6G	2.00	6.87
DHRS13	2.00	2.09
RAB9B	2.00	2.97

TABLE 4. Genes differentially expressed between non-thermogenic and thermogenic adipocytes that are maintained differentially expressed in WIM and TIM

Higher in thermogenic cells and TIM					Higher in non-thermogenic cells and WIM				
	Cells		Implants			Cells		Implants	
Gene	Fold Change	Log10 p-adj	Fold Change	Log10 p-adj	Gene	Fold Change	Log10 p-adj	Fold Change	Log10 p-adj
FER1L6	20.46	3.64	2.35	1.34	**ACHE**	14.06	61.50	1.39	1.71
TRIL	5.89	6.48	1.59	5.06	**GPAM**	8.12	25.75	1.43	2.28
DCHS1	5.59	19.37	1.46	1.56	**ACVR1C**	7.35	11.42	1.91	1.88
CACNA1G	4.33	7.21	2.24	1.56	**SLC2A4**	7.35	4.87	1.50	1.50
TGFB3	4.24	10.55	1.30	1.35	**ADH1B**	6.99	9.27	1.53	3.20
SLC7A8	3.95	15.07	1.68	3.10	**CALCRL**	4.94	15.96	1.68	3.89
ENC1	3.79	5.05	1.32	1.63	**FAM47E-STBD1**	4.30	4.75	1.29	1.34
DENND2A	3.71	4.74	1.46	1.87	**TRHDE**	4.20	31.23	1.56	2.01
IGF2	3.44	3.50	1.53	1.61	**GHR**	3.88	9.39	1.30	2.57
ELN	3.16	5.31	2.37	1.86	**FAM47E**	3.83	3.18	1.86	1.90
ADAM19	3.00	3.28	1.75	1.69	**APOE**	3.65	6.61	1.37	1.32
DDIT4	2.87	3.61	1.64	1.81	**RNF125**	3.49	6.17	1.94	1.56
SSC5D	2.81	79.00	1.50	1.99	**THBD**	3.44	3.23	2.96	1.41
COL12A1	2.75	3.95	1.56	2.26	**ANK3**	3.07	2.27	2.35	1.40
PLEKHG5	2.66	1.85	2.05	2.31	**ZNF117**	3.03	8.83	1.91	3.12
MRC2	2.65	19.93	1.43	2.52	**HK2**	2.91	14.26	1.28	2.75
CRABP2	2.59	6.22	1.67	3.20	**RGMB**	2.85	9.07	1.50	1.58
MMP14	2.58	5.30	1.60	3.99	**HLF**	2.66	1.82	1.93	4.21
NDRG2	2.49	4.08	1.38	2.48	**LRRC8C**	2.53	15.01	1.50	1.82
TNC	2.27	3.87	2.67	3.36	**KIAA0408**	2.51	3.88	1.53	2.16
NES	2.20	4.62	1.88	1.53	**MAOA**	2.50	13.88	1.31	2.25

GPX7	2.13	6.04	1.52	1.60

KLB	2.49	2.82	1.38	2.52
KIF21A	2.45	14.84	1.40	1.40
LRRC8B	2.38	22.44	1.87	3.85
LBHD1	2.32	6.93	2.41	4.99
CITED2	2.30	8.71	1.49	1.85
METTL7A	2.20	2.81	1.56	3.26
IL6ST	2.08	8.31	1.72	3.60
OSBPL8	2.07	8.58	1.60	2.57